frontiers | Frontiers in Water

TYPE Original Research
PUBLISHED 09 July 2025
DOI 10.3389/frwa.2025.1612232

OPEN ACCESS

EDITED BY
Amin Mojiri,
Arizona State University, United States

REVIEWED BY
Pragati Kumar,
Central University of Jammu, India
Tuan-Dung Hoang,
Vietnam National University, Hanoi, Vietnam

*CORRESPONDENCE
Mostafa R. Abukhadra
✉ abukhadra89@science.bsu.edu.eg
Basem E. Keshta
✉ basem.keshta@science.tanta.edu.eg
Mohamed Hamdy Eid
✉ mohamed.hemida@uni-miskolc.hu
Wail Al Zoubi
✉ wailalzoubi@ynu.ac.kr

RECEIVED 15 April 2025
ACCEPTED 09 June 2025
PUBLISHED 09 July 2025

CITATION
Al-Labadi IG, Horváth M, Alkilani AT, Al-Ma'abreh AM, Bashir MJK, Keshta BE, Hanbali G, Al Zoubi W, Abukhadra MR, Alqhtani HA and Eid MH (2025) Simultaneous adsorptive removal of Pb^{2+}, Cd^{2+}, Cu^{2+}, and Zn^{2+} using raw Norway Spruce biomass: a low-cost and eco-friendly solution for wastewater treatment.
Front. Water 7:1612232.
doi: 10.3389/frwa.2025.1612232

Simultaneous adsorptive removal of Pb^{2+}, Cd^{2+}, Cu^{2+}, and Zn^{2+} using raw Norway Spruce biomass: a low-cost and eco-friendly solution for wastewater treatment

Ibrahim G. Al-Labadi[1], Márk Horváth[1], Ayah T. Alkilani[2], Alaa M. Al-Ma'abreh[3], Mohammed J. K. Bashir[4], Basem E. Keshta[5,6]*, Ghadir Hanbali[7], Wail Al Zoubi[8]*, Mostafa R. Abukhadra[9,10]*, Haifa A. Alqhtani[11] and Mohamed Hamdy Eid[10,12]*

[1]Department of Environmental Analysis and Technologies, Institute of Environmental Sciences, Hungarian University of Agriculture and Life Sciences, Gödöllő, Hungary, [2]Department of Nutrition, Faculty of Pharmacy and Medical Sciences, University of Petra, Amman, Jordan, [3]Department of Chemistry, Faculty of Science, Isra University, Amman, Jordan, [4]School of Engineering and Technology, Central Queensland University, Melbourne, QLD, Australia, [5]Chemistry Department, Faculty of Science, Tanta University, Tanta, Egypt, [6]Key Laboratory of Ministry of Education for Advanced Catalysis Materials, Zhejiang Normal University, Jinhua, China, [7]Department of Chemistry, Faculty of Science, An-Najah National University, Nablus, Palestine, [8]Materials Electrochemistry Laboratory, School of Materials Science and Engineering, Yeungnam University, Gyeongsan, Republic of Korea, [9]Applied Science Research Center, Applied Science Private University, Amman, Jordan, [10]Materials Technologies and Their Applications Lab, Geology Department, Faculty of Science, Beni-Suef University, Beni-Suef, Egypt, [11]Department of Biology, College of Science, Princess Nourah bint Abdulrahman University, Riyadh, Saudi Arabia, [12]Institute of Environmental Management, Faculty of Earth Science, University of Miskolc, Egyetemváros, Hungary

This study evaluated the unmodified Norway Spruce Wood Residue (NSWR), an abundant lignocellulosic biomass, for the simultaneous removal of Pb^{2+}, Cd^{2+}, Zn^{2+}, and Cu^{2+} from a quaternary aqueous system. A series of batch adsorption experiments were performed to assess the influence of key operational parameters (pH, contact time, adsorbent dose, temperature, particle size, initial concentration), with equilibrium data subsequently fitted to Langmuir and Freundlich isotherm models, and the NSWR characterized using FTIR and EDS analyses. The results demonstrated maximum Langmuir adsorption capacities following the order Pb^{2+} (10.3 mg/g) > Cu^{2+} (7.9 mg/g) > Cd^{2+} (6.3 mg/g) > Zn^{2+} (6.0 mg/g), corresponding to high removal efficiencies (up to 99% for Pb^{2+}). Adsorption was rapid initially (~60% removal within 20 min) and favored slightly acidic conditions (pH 5–6) and moderately elevated temperatures (45°C). The Langmuir model provided an excellent fit to the data ($R^2 \approx 0.99$), indicating favorable monolayer chemisorption, likely driven by a combination of cation exchange supported by EDS and interactions with surface functional groups. Conclusively, unmodified NSWR shows significant promise as an effective, inexpensive, and eco-friendly biosorbent for treating water contaminated with multiple heavy metals, presenting a viable waste valorization strategy for sustainable water management.

KEYWORDS

adsorption, heavy metals, karst biomass, lignocellulosic biomass, Norway Spruce wood residue, *Picea abies* (L.)

1 Introduction

Toxic heavy metal contamination of water resources is a pressing global issue, threatening millions of lives and impacting aquatic ecosystems(Keshta et al., 2024; Hussain et al., 2025; Khedulkar et al., 2025), thereby hindering the achievement of Sustainable Development Goals (SDGs) (Ofudje et al., 2023). Heavy metals (HMs) such as Cadmium (Cd), Copper (Cu), Lead (Pb), Mercury (Hg), Arsenic (As), and Zinc(Zn), with densities exceeding (5 g/cm^3) are classified as potentially toxic elements (PTEs) due to their potentially hazardous effects (Armaya'u et al., 2024; Javeria et al., 2025; Soni et al., 2025; Ali et al., 2023). The World Health Organization (WHO) designated permissible levels in µg/L for Pb, Zn, Cu, and Cd in drinking water are (100, 3,000, 1,000, and 10) respectively (Abdulkareem et al., 2023). Contaminated drinking water causes approximately 2.2 million deaths annually (Rind et al., 2024). Over 40% of global lakes and rivers are polluted with HMs. HMs exhibit high solubility, persistence, and toxicity, accumulating in living tissues and ecosystems (Hao et al., 2024). The reason behind choosing the 4 HM ions, i.e., (Pb, Zn, Cu, and Cd) in this work was determined based on research conducted by Wang and co-authors. They found that the complex (Cd-Pb-Zn) often occurs together in nature (Wang et al., 2024).

Given the increasing water pollution, researchers have explored methods such as phytoremediation, reverse osmosis, membrane filtration, and electrochemical treatments to remediate contaminated water (Keshta et al., 2023; Zhu et al., 2024). However, these approaches can be costly, produce hazardous sludge, and may be ineffective at low metal concentrations (Mishra et al., 2024). Biosorption, using lignocellulosic biomass (LCB) and agricultural waste, has emerged as a cost-effective and efficient alternative for HM removal (Zhu et al., 2024; Soni et al., 2025). Various types of agricultural wastes such as sugarcane bagasse, rice husk, coconut shell, and coconut husk were used for the elimination of HMs from polluted water (Mathew et al., 2016). Global agricultural by-products usually go to waste, especially in developing countries where agricultural products are usually exported as raw products. Such waste streams, once converted to "value-added" products, could be an additional source of revenue while simultaneously having positive impacts on the socio-economic well-being of local people, promoting sustainable environmental practices (Hoang et al., 2024). These waste materials possess enriched surface functional groups, a porous structure, and a large specific area, remarkable thermal and chemical stabilities all of which make them potential adsorbents for different pollutants. Besides, it is noteworthy that most biosorbents derived from agricultural waste could be used directly in their raw state (without modification) (Kainth et al., 2024; Sánchez-Moreno et al., 2025) Lignocellulose (LC), the most abundant biomass on Earth, stands out among the many possibilities as the most appealing possibility for water cleanup. LC is also ranked as the third largest energy source globally (Liu et al., 2015; Abi Bianasari et al., 2024; Uddin et al., 2024). Besides, it effectively adsorbs a range of pollutants, from HMs to organic contaminants, with minimal environmental impact (Bhardwaj et al., 2025). Compared to conventional methods, biosorption can reduce treatment costs by up to 20% (Fertu et al., 2022). Despite extensive research on mono-element adsorption, studies on multi-element systems remain limited, even though real wastewater (WW) contains complex mixtures of metals (Chen et al., 2022). The presence of multiple ions in WW can cause competitive and antagonistic interactions, influencing adsorption mechanisms (Kothavale et al., 2023).

Furthermore, most studies focus on chemically modified biosorbents, neglecting the potential of unaltered, low-cost alternatives. There is also a lack of research on how key operational parameters such as pH, stirring speed, and temperature affect biosorption in multi-metal systems (Jiang et al., 2024). Addressing these gaps is crucial to developing efficient and scalable water treatment solutions. This study investigates the potential of NSWR as a promising renewable, affordable, and biodegradable biosorbent for simultaneous (Cd, Cu, Pb, and Zn) removal in a four-element synthetic WW system. This affordability makes NSWR an attractive alternative to synthetic adsorbents like activated carbon, which can be expensive and resource-intensive to produce. The performance of NSWR is evaluated based on seven factors: adsorbent dose, contact time, stirring speed, temperature, particle size, initial ion concentration, and pH. To minimize costs and environmental impact, NSWR is used in its raw state. This research contributes to developing sustainable water treatment solutions while addressing agricultural waste management challenges.

2 Materials and methods

2.1 Materials

A specimen of Norway Spruce wood chips with the scientific name *Picea abies (L.) Karst*. was used as mulching material and was acquired from an agricultural firm located in Godollo, Hungary.

2.2 Adsorbent preparation method

The raw sample of Norway Spruce was thoroughly rinsed with ddH_2O to expel any potential contaminants, i.e., soil bits, adsorbed salts, or soluble dirt, and to decrease the concentration of free electrolytes. The rinsed sample was dried at room temperature for 24 h and then dried in an oven: WTB binder 7,200, Tuttlingen, Germany, at 85°C for 48 h to prevent any microbial activity. Finally, the dried specimen was crushed into powder using an IKA MF 10 basic Microfine grinder. The powdered material was duly sieved and thereafter stored in hermetically sealed containers within the desiccator manufactured by Thermo Fisher Scientific–US.

2.3 Solution preparation

A stock solution of 1,000 mg/L (Pb^{2+}, Cu^{2+}, Zn^{2+}, and Cd^{2+}) was prepared using ultrapure analytical-grade salts obtained from Merck (Germany). The working solutions of HM ions were prepared by appropriate dilutions immediately before their use. The calculated masses of these salts were dissolved in a volumetric flask having a 0.01 (mol/L) Sodium Nitrates ($NaNO_3$) solution to simulate the ionic strength (I) of industrialized WW. To achieve complete dissociation of the HM ions involved in the solution and prevent hydrolysis, a small amount of 68% nitric acid (HNO_3) was introduced. Subsequently, the flask was capped, labeled, and vigorously stirred for 25 min via a Stuart CB162 hotplate stirrer. The initial solution was then prepared in various doses, fluctuating from 1 to 100 mg/L. The study utilized double-distilled water (ddH_2O)

10.3389/frwa.2025.1612232

generated by the Merck Milli Q ultra-pure water purification system, which has an electrical resistance of 18.2 MΩ × cm at a temperature of 25°C. To eliminate any potential origin of previously attached HM, all the glassware used in this study was immersed in HNO_3 overnight and thereafter rinsed meticulously with ddH_2O before being utilized.

2.4 Batch adsorption experiments

To determine the impact of pH, mixing time, HM particle size, temperature, stirring speed, and adsorbent mass on the adsorption procedure using (NSWR), sequences of controlled batch experiments were done. Batch studies were conducted by agitating a predetermined amount of NSWR and 50 ml of the chosen concentration of the quaternary-metal systems (Cd^{2+}, Cu^{2+}, Pb^{2+}, and Zn^{2+}) in 250 ml sealed Erlenmeyer flasks in a temperature-controlled shaker GFL 1083 rotating water bath at a speed of 200 rpm. The temperature ranged from 25.6 to 26.2°C. The particle size of NSWR was calibrated to a range of 90–250 µm unless the Impact of particle size was examined. To inspect the impact of temperature on adsorption, 5 different temperature levels (25–45°C) were randomly assigned. The influence of stirring speed was investigated by manipulating the stirring speed within the range of 40 to 400 rpm via the New Brunswick Scientific Gyratory shaker model G2, US. The pH levels were tuned to 9 distinct values (2–6) via tinned solutions of HNO_3 and NaOH. After acidifying with HNO_3, the supernatant of all the samples was passed through 0.45 mm Whatman filter papers that had been pre-saturated with ddH_2O. The collected solutions were then placed in 10 ml labeled plastic centrifuge tubes and securely kept in track tubes in the laboratory's fridge. The analysis was done within a max. of 2 days. The remaining concentrations of HM ions in the supernatant solutions were analytically determined via the Inductively Coupled Plasma-Optical Emission Spectrometer (ICP-OES) model (Horiba Jobin Yvon Activa-M). The used biosorbent powder was desiccated and stored for further scientific investigation. All the analyses were conducted in triplicate to ensure the authenticity and consistency of the acquired investigational findings were met.

Furthermore, controls were also employed for the goal of quality control. The mean results of the three triplicates were taken, and the maximum. Standard Deviation was set at 5%. Typically, the max. sorption capacity and "HM eviction% %" are commonly the primary parameters used to quantitatively assess the practical application capability of different biomass adsorbents. The adsorption capacity (mg/g) was calculated via Equation 1:

$$q = \left[\left(C_i - C_f\right) * V\right] / M \quad (1)$$

The variables in the equation are as follows: q represents the adsorption capability (mg/g), Ci represents the primary doses of metal in solution (mg/L), Ce represents the equilibrium doses of metal in solution (mg/L), V represents the volume of HM ion solution (in liters), and M represents the mass of the biosorbent (in g).

Removal percentage (R%) was expressed by employing Equation 2:

$$R(\%) = \left(\left(C_i - C_f\right) / C_i\right) * 100 \quad (2)$$

C_i is the preliminary dose of metal in solution (mg/L), and C_e is the equilibrium dose of metal in solution (mg/L). The above-mentioned Equations 1 and 2 were taken from Xu et al. (2024).

2.5 Adsorption isotherm

Adsorption equilibrium is one of the most important parameters required for the adequate analysis and design of the adsorption process. It gives us specific information about the adsorption mechanism, surface properties, and the affinity of the adsorbent for specific HM ions (Mosoarca et al., 2020). In this study, the most common linear adsorption isotherm models, Freundlich and Langmuir, have been applied. These two isotherm models are the most widely used isotherms for the biosorption of a solute from a liquid solution. (Table 1) provides these two adsorption models' equations, main findings, and parameters.

2.6 Characterization of NSWR

To assess the physical and chemical properties of NSWR as a biosorbent and to aid in elucidating the potential mechanisms involved in HMs adsorption, a suite of analytical techniques was employed.

2.6.1 Elemental analysis (C, H, N, S)

The bulk elemental composition (Carbon, Hydrogen, Nitrogen, Sulfur) of the prepared NSWR powder was determined using a Perkin Elmer 2400 SERIES-II CHNS/O analyzer. Oxygen content was typically calculated by differences.

2.6.2 Initial heavy metal content

To establish baseline levels, the inherent concentrations of the target HMs [(Cd), (Cu), (Pb), and (Zn)] in the raw NSWR sample were quantified. This analysis was performed using Inductively

TABLE 1 Linear and nonlinear adsorption isotherm models.

Isothermal model	Linear equation	Parameters
Langmuir (1918)	$\frac{C_e}{q_e} = \frac{1}{k_L q_m} + \frac{C_e}{q_m}$ … [7]	q_e: is the equilibrium quantity of the adsorbate (mg/g). C_e: is the equilibrium concentration of the adsorbate (mg/L). K_L: the constant of Langmuir isotherm. q_m: is the adsorption capacity (mg/g)
Freundlich (1906)	$\log q_e = \log K_f + \frac{1}{n}\log C_e$ [8]	K_f: the Freundlich isotherm constant, measured in units of mg/g. N denotes the adsorption intensity.

Coupled Plasma-Optical Emission Spectrometry (ICP-OES, Horiba Jobin Yvon Activa-M) following sample digestion.

2.6.3 Crystalline structure (XRD)

The phase composition and degree of crystallinity of the NSWR were examined using X-Ray Diffraction (XRD). Analyses were carried out on a Bruker D4 Endeavor X-Ray Diffractometer (Germany). The instrument was configured with CuKα radiation (λ = 1.54056 Å) and operated at a voltage of 40 kV and a current of 30 mA (Power = 1.8 kW). Diffractograms were recorded over a 2θ angular range from 5 to 70°, utilizing a step size of 0.02° and a data acquisition time of 1 s per step.

2.6.4 Functional group analysis (FTIR)

The identification of surface functional groups presents on the NSWR, which may serve as binding sites for HM ions, was achieved using Fourier Transform Infrared (FTIR) spectroscopy. Spectra were acquired using a Bruker Vertex 70v spectrometer equipped with an Attenuated Total Reflectance (ATR) sampling accessory. Scans were performed over the wavenumber range of 4,000–400 cm^{-1} with a resolution of 4 cm^{-1} and accumulating 32 scans for signal averaging.

2.6.5 Surface morphology and microanalysis (SEM/EDS)

The surface topography and morphological features of the NSWR particles, both in their initial state and after being loaded with HMs during adsorption experiments, were visualized using Scanning Electron Microscopy (SEM). Thermo Scientific Phenom XL G2 Desktop SEM was employed for this purpose. Images were typically captured using a Backscattered Electron Detector (BSD) under low vacuum conditions (approximately 10 Pa) with an electron beam accelerating voltage of 10 kV at various magnifications as required (e.g., 650x, 1,000x). Concurrently, semi-quantitative elemental analysis of the sample surface was performed using energy-dispersive X-ray Spectroscopy (EDS) integrated with the SEM system.

2.6.6 Surface area and porosity (BET)

The specific surface area, total pore volume, and average pore width of the NSWR biosorbent were determined based on nitrogen gas adsorption–desorption isotherms measured at 77 K. The analysis was performed using a Micromeritics Gemini VII 2390 t Surface Area and Porosity Analyzer. The specific surface area was calculated using the Brunauer–Emmett–Teller (BET) method from the adsorption data in the relative pressure (P/P_0) range of 0.05–0.35. Total pore volume was estimated from the amount of nitrogen adsorbed at a relative pressure close to unity (e.g., $P/P_0 \approx 0.99$).

2.6.7 Point of zero charge (pH_{pzc})

The point of zero charge (pH_{pzc}), representing the pH value at which the net surface charge of the NSWR material is neutral, was determined using the pH drift method. Briefly, fixed amounts of NSWR were added to a series of solutions with known initial pH values (typically ranging from 2 to 10), adjusted using dilute NaOH. The suspensions were agitated until equilibrium was reached (e.g., 24–48 h), and the final equilibrium pH was measured. The pH_{pzc} was identified as the point where the plot of final pH versus initial pH intersects the line of final pH = initial pH or where the plot of ΔpH (final pH - initial pH) versus initial pH crosses the zero ΔpH axis.

2.6.8 Thermogravimetric analysis (TGA) and differential scanning calorimetry (DSC)

The thermal stability of NSWR sample and the corresponding changes in its mass were carried out by (TGA) and (DSC) analysis using Netzsch-Gerätebau GmbH - STA 409 PC Luxx Simultaneous thermal analyzer, with dynamic nitrogen atmosphere (gas flow of 50 ml min^{-1}), between 80 and 6,497°C with Heating and cooling rates: 5 K/min to 20 K/min, 5.2 mg ± 0.1 mg sample.

3 Results and discussion

3.1 Biosorbent characterization

The physicochemical properties of the (NSWR) were thoroughly investigated to understand its suitability as a biosorbent for HMs.

3.1.1 Bulk composition and inherent properties

NSWR, as a lignocellulosic biomass, derives its properties from its chemical makeup and physical structure (Bhardwaj et al., 2025). Chemically, it is primarily organic, composed mainly of cellulose, hemicellulose, and lignin (Miranda et al., 2012; Basit et al., 2024; Yi et al., 2024). This was reflected in the elemental analysis conducted in this study, which showed high proportions of Carbon (43.46%), Oxygen (50.86%), and Hydrogen (5.52%). Proximate analysis of Spruce (*Picea abies*) further characterized the material with a volatile content of 80.2 ± 1.11%, fixed carbon content (17.63 ± 0.45%), moisture content (8.60 ± 0.2) and ash content (0.39 ± 0.07) as reported by Awan et al. (2024) and Matin et al. (2024).

Background levels of the target HMs (Cd, Cu, Pb, Zn) were measured in the sample prepared to assess potential interference. As detailed in Table 2, these inherent concentrations were found to be low.

3.1.2 Crystalline structure

The XRD diffractogram of unmodified (Figure 1) confirms its predominantly amorphous nature, characterized by a broad diffraction halo spanning 2θ ≈ 15–22°, consistent with the disordered structure of cellulose and lignocellulosic materials (Ivanovska et al., 2021). Minor crystalline phases are evident as sharp peaks at 2θ = 26.6° and 36.5°. The peak at 26.6° is indexed to the (101) plane of quartz (SiO_2), aligning with JCPDS No. 00–046-1045 (Deka and Maji, 2013), a common impurity observed in wood-derived materials. The peak at 36.5° is tentatively attributed to calcite ($CaCO_3$), corresponding to the (104) plane (JCPDS No. 00-005-0586; Zhang et al., 2022). These findings corroborate with prior studies reporting similar diffraction patterns in aged lignocellulose fibers and carbonized wood, underscoring the material's inherent heterogeneity. The presented pattern shows a well-resolved characteristic peak with the highest

TABLE 2 Cd^{2+}, Cu^{2+}, Pb^{2+}, and Zn^{2+} masses in the crude sample (NSWR).

Elements	Unit (mg/g)
Cd^{2+}	0.00028
Cu^{2+}	0.0096
Pb^{2+}	0.0047
Zn^{2+}	0.022

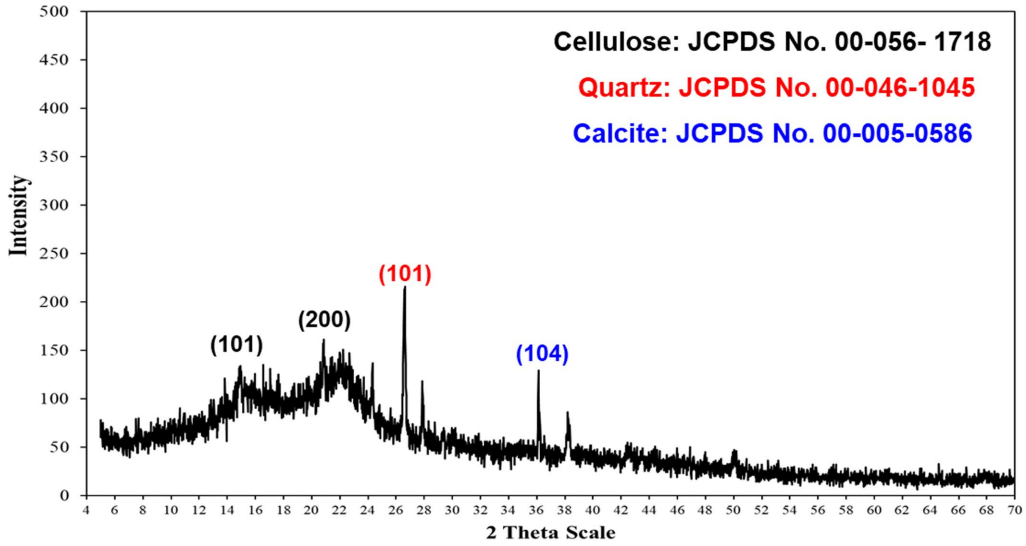

FIGURE 1
XRD pattern of NSWR.

intensity obtained at a value of around 21° corresponding to the (200) plane for cellulose, thus indicating an amorphous cellulose type I. The obtained peak was broad and not sharp, which is typical for amorphous substances since they do not possess a long range of Bragg peaks in X-ray diffraction order. This data further confirmed FTIR analysis that showed cellulose as the main constituent of the used NSWR biosorbent (Figure 1), with functional groups having bonding affinity toward HM ions in aqueous solutions. The same findings were obtained from Šehović et al. (2022) on lignocellulosic biomass of *Citrus limon* peel as a biosorbent for the removal of Cr^{3+}, $Cu^{2+,}$ and Pb^{2+} ions. Overall, the XRD analysis validates NSWR's suitability as a low-crystallinity adsorbent for HM ions while highlighting the need for deeper characterization of trace mineral phases.

3.1.3 Surface functional groups (FTIR)

The FTIR spectrum of NSWR (Figure 2) exhibits several absorption bands indicative of its lignocellulosic composition. A broad band centered around 3,330 cm^{-1} corresponds to O-H stretching vibrations from hydroxyl groups (in cellulose, lignin, and adsorbed water). Peaks at approximately 2,920 and 2,854 cm^{-1} are attributed to C-H stretching vibrations in aliphatic chains. The prominent peak at 1,605 cm^{-1} can be assigned to C=C aromatic ring vibrations in the lignin and possibly overlapping contributions from adsorbed water-bending vibrations. The band at 1513 cm^{-1} is also characteristic of lignin aromatic skeletal vibrations. The region between 1,450 cm^{-1} and 1,200 cm^{-1} < contains multiple peaks related to C-H bending and C-O stretching vibrations (Abou-Elyazed et al., 2024; Yi et al., 2024). A very strong and broad absorption band dominating the spectrum is centered near 1,025 cm^{-1}, characteristic of C-O stretching and C-O-C ether linkages prevalent in cellulose and hemicellulose polysaccharides (Armaya'u et al., 2024; Uddin et al., 2024). The presence of these diverse oxygen-containing functional groups (hydroxyl, carboxyl/carbonyl - implied by C=O near 1,605 or potential weak shoulder near 1730, ether suggests multiple potential binding sites for heavy metal cations.

3.1.4 Surface morphology

SEM micrographs reveal the surface morphology and the porous structure of NSWR before and after HMs adsorption (Figures 3). Prior to adsorption (Figure 3A, 1,000×), the material displays a heterogeneous and irregular surface structure, characterized by rough textures, fragmented particles, and evidence of a relatively porous feature. After exposure to the HMs solution (Figure 3B, 650×), the holes were filled with the HM ions, the surface heterogeneity declined, and the pores appeared to be smooth. These characteristics indicate a high ability for biosorption of HMs. The same findings were obtained by applying *Meretrix lusoria* biosorbent for removing Cd^{2+} and Pb^{2+} ions (Al-Mur, 2024).

3.1.5 Surface elemental composition (EDS)

EDS analysis was conducted to identify the elements present on the NSWR surface, particularly after adsorption. A representative spectrum of the metal-loaded NSWR is shown in Figure 4. The spectrum confirms the presence of distinct peaks corresponding to the targeted HMs (Pb), (Cu), (Cd), and (Zn) are clearly visible, confirming their successful adsorption onto the biosorbent surface. The corresponding values of the wt. % of the HM ions reflect their affinities arrangement to NSWR. Additionally, elements such as Calcium (Ca), Sulfur or Sulphur (S), Phosphorus (P), and Aluminum (Al) were detected, likely to originate from the inherent composition of the wood biomass (Figure 4), which probably originate from substances absorbed by the tree in the soil (Salamat et al., 2017). Semi-quantitative results from EDS analysis are presented in Table 2. The presence of cations (especially Ca^{2+}) reinforces the potential role of ion exchange in the adsorption and hydrogen bond formation mechanisms. This interesting role of such ions in adsorption is consistent with literature findings (Šehović et al., 2022).

3.1.6 Surface area and porosity (BET)

Quantitative surface analysis using N_2 adsorption provided the parameters detailed in Table 3.

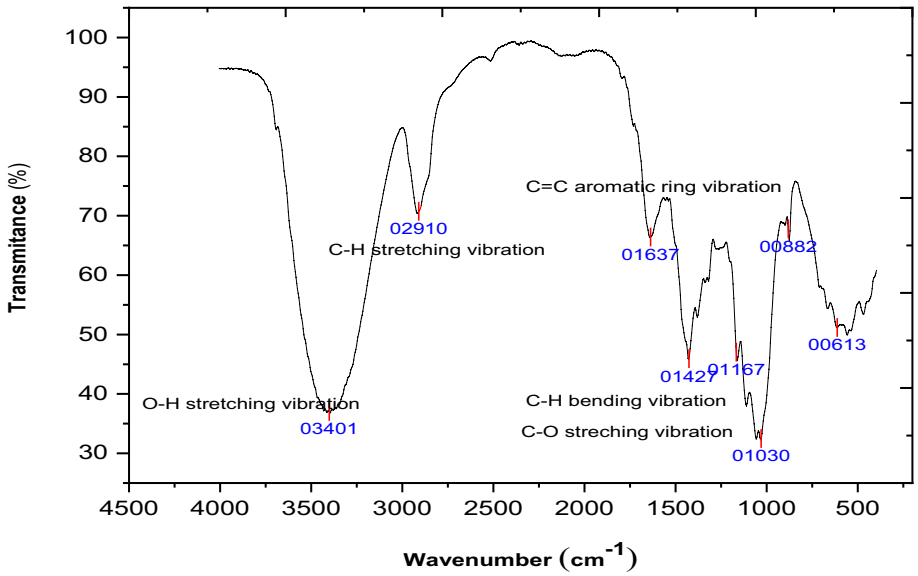

FIGURE 2
FTIR spectrum of NSWR.

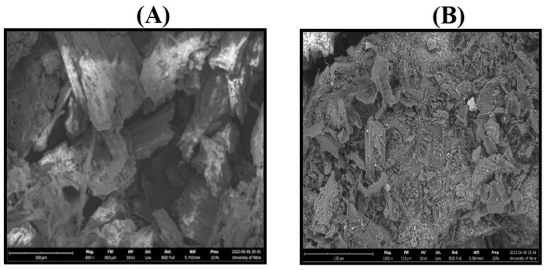

FIGURE 3
SEM Micrographs of NSWR: **(A)** Before adsorption, **(B)** After adsorption.

The NSWR exhibited a BET-specific surface area of 4.5630 m^2/g and a total pore volume of 0.00532 cm^3/g. While the surface area is modest, the average pore width of 46.655 Å suggests a predominantly mesoporous character, potentially facilitating access to internal binding sites. Likewise, similar findings were obtained using *Abies bornmulleriana* cones for the removal of Pb, Cu, Cd, Ni, and Co ions. The BET surface area and pore volume of the biosorbent were defined to be 5.05 m^2/g and 0.0018 cm^3/g. The average pore width of the biosorbent used in that study was calculated to be 9.34 (Oguz, 2020).

3.1.7 Point of zero charge (pH_{pzc})

The point of zero charge (PZC) is almost obligatory in the characterization of adsorbents (Kosmulski, 2023) because the surface charge behavior of NSWR is crucial for electrostatic interactions. The point of zero charge (pH_{pzc}) was determined to be 5.7 (Figure 5). This indicates the pH at which the net surface charge is neutral; above (pH_{pzc}), electrostatic repulsion occurs, reducing metal cation adsorption above this (pH_{pzc}), the surface becomes increasingly negative, enhances electrostatic attraction thus, favoring and facilitating cation adsorption (Al-Labadi et al., 2023).

3.1.8 TGA and DSC analysis

Both DSC and TGA analyses were conducted on the adsorbent material (NSWR). The results are shown in Figures 6A,B. The DSC thermogram (Figure 6A) reveals a significant exothermic event, indicating thermal decomposition or a phase transition in the sample. The process begins at an onset temperature of 145.0°C, suggesting the thermal stability is up to this point. The maximum thermal activity occurs at (369.7°C), marking the peak of decomposition or structural transformation, and the process concludes at (298.2°C). The broad peak width of 210.7°C, spanning 37% of the temperature range, suggests a complex reaction mechanism, potentially involving overlapping transitions or multiple degradation steps. As indicated by the peak area (228.2 μV·s/mg), the total energy involved reflects a high-energy reaction. These results provide insight into the material's thermal behavior, highlighting its stability range and the energy dynamics of its decomposition process, which are critical for applications requiring thermal stability or controlled degradation.

The TGA thermogram (Figure 6B) shows a slight weight loss was detected between (30 to 110°C) which was attributed to the removal of moisture content and light volatile compounds, while a mass loss of 43.05%, indicating a significant thermal decomposition process occurring between 145 and 369.7°C. This range aligns closely with the exothermic event observed in the DSC thermogram, confirming that the mass loss is due to decomposition or structural breakdown of the material.

The stable region before (145°C) reflects the material's thermal stability, consistent with the onset of the DSC peak. The correlation between the TGA and DSC results highlights that the observed energy release in the DSC is directly related to the decomposition process evidenced by the mass loss in the TGA, suggesting a strong link between the thermal stability and degradation mechanisms of the

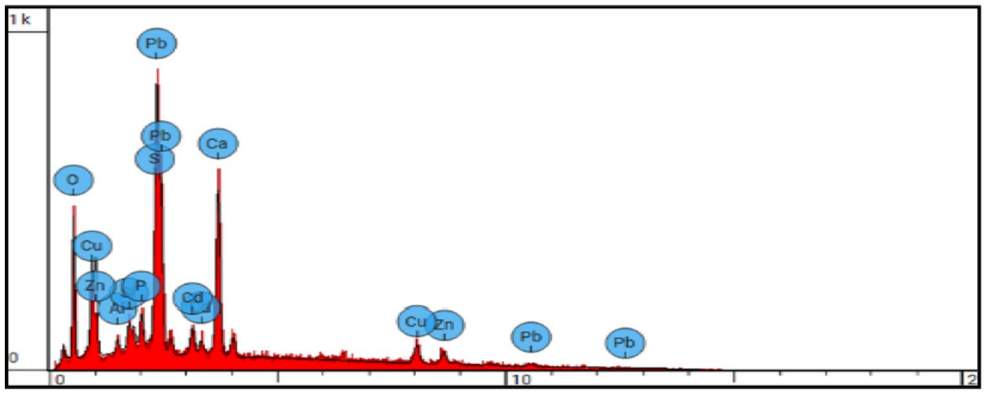

FIGURE 4
Representative EDS spectrum of NSWR after heavy metal adsorption.

TABLE 3 The BET surface area analysis of NSWR.

BET surface area (m^2/g)	4.5630
Total pore volume (cm^3/g)	0.00532
Adsorption average pore width (4 V/A by BET) (Å)	46.655
Langmuir surface area (m^2/g)	7.192
Single point surface area at p/p_0 (m^2/g)	4.429

material. This thermal stability can be considered a good property of NSFR as an efficient candidate adsorbent for HM removal.

3.2 Adsorption mechanism

The adsorption of HM ions onto wood biomass is influenced by multiple interacting factors, including solution properties (temperature, pH, competing ions) and the physicochemical characteristics of both the sorbent and the metal species (Singh et al., 2022). Lignocellulosic biosorbents, like NSWR, are often effective due to their porous structure, relatively large surface area (although the specific area can vary greatly), and diverse surface functional groups, which facilitate metal binding (Bhardwaj et al., 2025).

The mechanisms responsible for Heavy Metal (HM) removal by biomass have been extensively studied. For hardwood sawdust, surface complexation, and ion exchange were identified as primary pathways (Kovacova et al., 2020). In contrast, research specifically on spruce sawdust highlighted the dominance of ion exchange (Marin and Ayele, 2002). These studies suggest that acidic functional groups on the biomass surface can release protons, which are subsequently replaced by HM ions. This process often involves the participation of naturally present cations such as Ca^{2+}, Mg^{2+}, Mn^{2+}, and K^+ in HM sequestration, a finding supported by recent work confirming the importance of these inherent ions in facilitating ion exchange (Orozco et al., 2023). A range of mechanisms can contribute to the overall biosorption process, potentially including chemisorption, complexation, ion exchange, microprecipitation, surface adsorption, and complexation within pores (Demirbas, 2008).

Biosorption mechanisms using okara-based biosorbent for Cd^{2+} removal were attributed to ionic exchange, hydrogen bonding, and electrostatic interactions (Hiew et al., 2021). The spectroscopic and microscopic analyses performed in this study provide insights into the structural attributes of NSWR influencing adsorption. FTIR spectra (Figure 2) confirmed the presence of key functional groups abundant in lignocellulose, such as hydroxyl (O–H), aliphatic (C–H), and various oxygen-containing moieties (including C-O and likely carbonyl groups). These groups are known to participate in metal ion binding through mechanisms like hydrogen bonding, electrostatic interactions, and surface complexation (Natrayan et al., 2022). Furthermore, EDS analysis after adsorption (Table 4; Figure 4) not only confirmed the uptake of the target HMs but also revealed the significant presence of inherent Ca ions alongside Si on the NSWR surface. This strongly reinforces the likely contribution of ion exchange involving native cations (like Ca^{2+}) in the HMs adsorption process (Simón et al., 2022). The SEM images (Figure 3) highlighted NSWR's heterogeneous morphology, characterized by a rough, irregular surface with protrusions and folds. These structural features enhance the accessibility of the surface for interaction between the adsorbent and the HM ions, contributing to adsorption efficiency (Božić et al., 2009).

Further structural context is provided by the XRD analysis (Figure 1), which confirmed the predominantly amorphous lignocellulosic nature of NSWR, with evidence of minor crystalline inorganic phases. Crystalline materials, with their ordered frameworks and uniform pore sizes, enable selective gas separation by restricting molecular access to adsorption sites based on size and structure (Chen et al., 2025; Xu et al., 2025). Meanwhile, the interplay between amorphous and crystalline domains in heterostructures further optimizes adsorption efficiency, leveraging the complementary strengths of both phases. Amorphous materials, on the other hand, typically have a more disordered pore structure with a wider distribution of pore sizes, allowing for better accessibility and accommodation of adsorbates. The physicochemical heterogeneity found on amorphous surfaces leads to a complex interaction of adsorbate molecules with topological and undercoordinated defects, which enhance the adsorption capacity and can participate in catalytic reactions (Turchi et al., 2024). Conversely, the open pore structure of

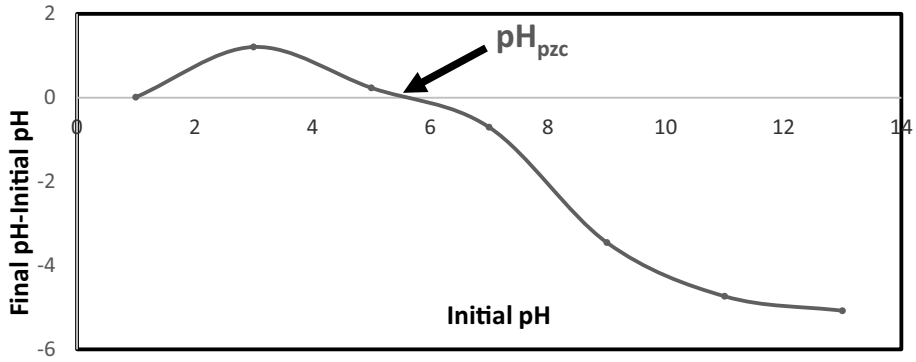

FIGURE 5
The point of zero charge (pH_{PZC}) for NSWR.

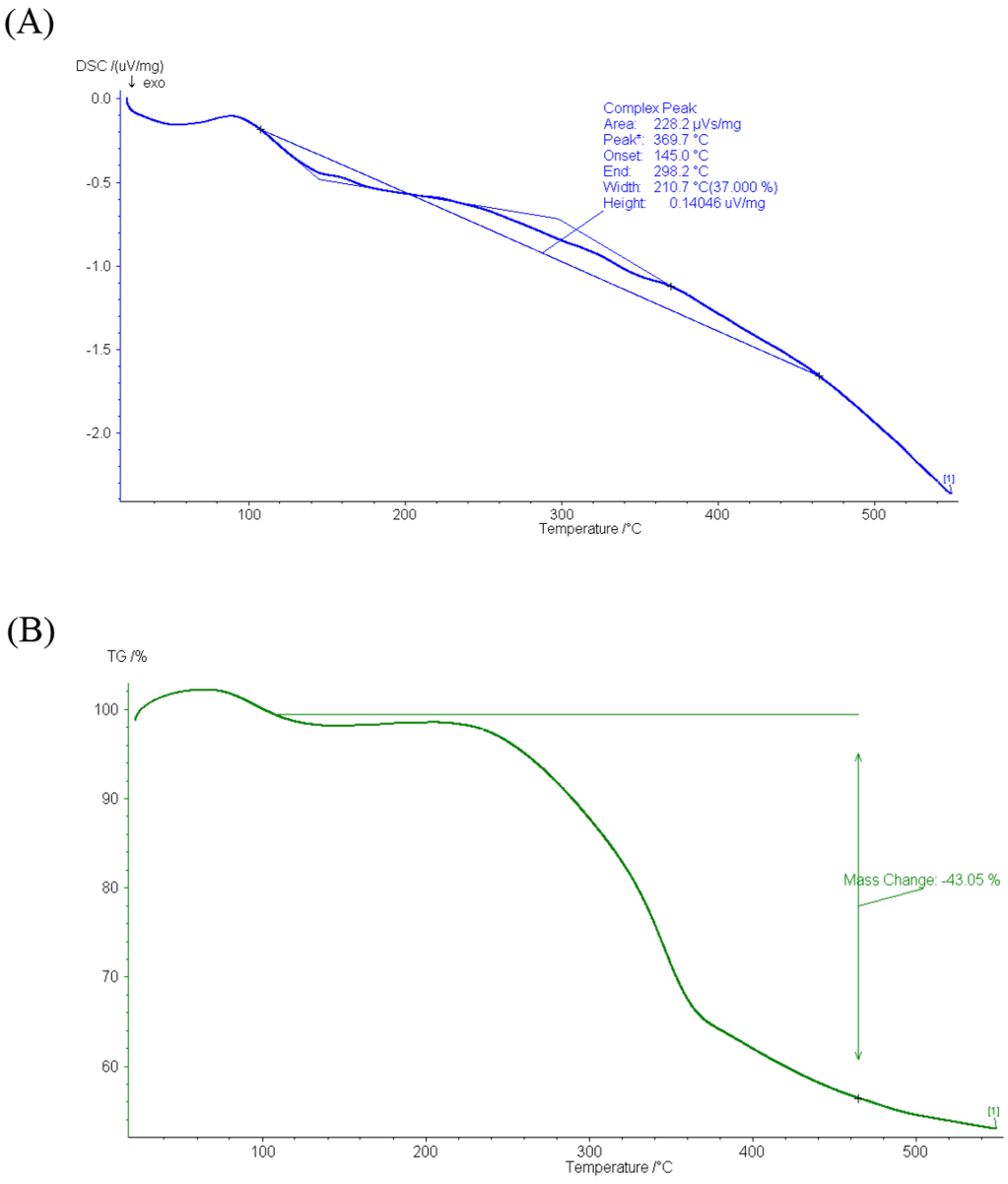

FIGURE 6
(A) DSC analysis and **(B)** TGA analysis for NSWR.

10.3389/frwa.2025.1612232

TABLE 4 EDS analysis of NSWR.

Element No.	Element Symbol	Element Name	Atomic Conc.	Weight Conc.
8	O	Oxygen	46.47	14.49
13	Al	Aluminium	1.33	0.70
14	Si	Silicon	1.46	0.80
15	P	Phosphorus	2.65	1.60
16	S	Sulfur	1.92	1.20
20	Ca	Calcium	20.47	15.98
29	Cu	Copper	7.91	9.79
30	Zn	Zinc	3.92	5.00
48	Cd	Cadmium	3.01	6.59
82	Pb	Lead	10.86	43.86

ordered mesoporous materials facilitates better target molecule access and transfer than bottleneck pores of amorphous materials, which impede molecular passage to the adsorption sites, as stated by Ezzeddine et al. (2025). Compared to conventional absorbents, molecule-based crystalline materials show the advantages of extremely rich and easily designable/synthesized/characterized structures as well as remarkable flexibility.

Although amorphous materials might possess better adsorption capabilities compared to crystalline ones, other influencing parameters controlling the adsorption process like pH, surface functional groups, design, synthesis, characterization, and the type of adsorbate must all be considered. Hence, an in-depth study is needed to comprehensively understand the effect of amorphous and crystalline nature.

The potential presence of mineral phases like SiO_2 (quartz) and $CaCO_3$ (calcite), suggested by minor XRD peaks, could offer additional sites or mechanisms for interaction with HM ions (Ivanovska et al., 2021). Despite NSWR exhibiting a relatively low BET-specific surface area (4.5630 m^2/g, Table 4), its adsorption capacity is not solely dependent on this parameter. Instead, the ampleness and accessibility of surface functional groups (identified by FTIR), combined with the overall structural characteristics (morphology, porosity, presence of exchangeable cations), appear to be significant factors driving metal binding efficiency (Akpomie et al., 2023; Mo et al., 2023).

3.3 Parametric impacts

3.3.1 Impact of the biosorbent amount

The mass of the biosorbent is an important determinant of the absorption measurements for a particular ion concentration. It accurately determines the ideal absorbent mass required to absorb the most metal cations under a certain set of configurable parameters.

Adjusting the mass of the biosorbent is necessary to choose the most economical amount to be employed. (Figure 7) illustrates the absorption efficiency (R%) of HMs for Cd^{2+}, Cu^{2+}, Pb^{2+}, and Zn^{2+} ions, concerning the mass of the biosorbent. As the adsorbent dosage increased from 0.005 to 0.1 g, the percentage of removal efficiency (R%) for Cd^{2+}, Cu^{2+}, Pb^{2+}, and Zn^{2+} ions each rose from 42.65 to 88.51%, 60.34 to 94.87%, 64.57 to 99.11, and 45.93 to 86.46%,

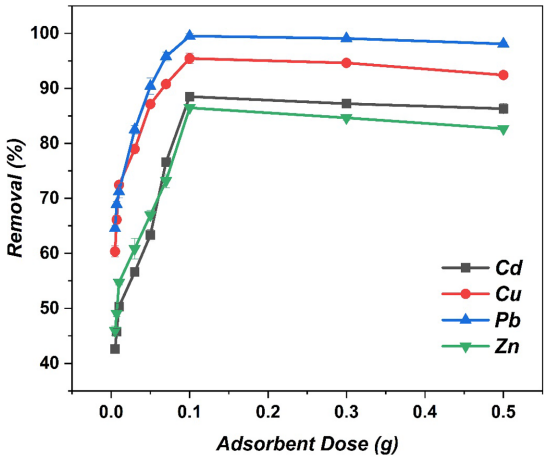

FIGURE 7
Impact of adsorbent doses (g) on the biosorption of Cd^{2+}, Cu^{2+}, Pb^{2+} and Zn^{2+} via NSWR (PH = 5–6 ± 0.1, 0.01 M $NaNO_3$, stirring speed = 200 rpm, particle size = 250–90 µm, HMs solution volume = 50 ml, initial HMs ions conc. of Cd^{2+}, Cu^{2+}, Pb^{2+} and Zn^{2+} = 50 mg/L).

respectively, in an orderly and accordingly in direct proportion. The increase in adsorption percentage with a dosage of adsorbent can be ascribed to the addition of more sorbent mass, namely a higher ratio of metal cations to binding sites, which leads to a greater number of accessible unsaturated or vacant active sites in the biosorbent. Consequently, the surface area of the sorbent also improves. Moreover, the highest level of biosorption for Cd^{2+}, Cu^{2+}, Pb^{2+}, and Zn^{2+} ions of the HMs ions was achieved at a biosorbent mass of 0.1 g/0.01 L, equivalent to 1 g/0.1 L. Further rises in the adsorbent mass above 0.1 g were found to have an inverse effect on the biosorption proportion. In the current investigation, a biomass dosage of 0.1 g/0.001 L was deemed optimal for further trials in this work.

3.3.2 Impact of time

The impact of the duration time on the absorption of Cd^{2+}, Cu^{2+}, Pb^{2+}, and Zn^{2+} ions was examined. Figure 8 shows that the sorption process occurred rapidly within the first 20 min, resulting in the deletion of approximately 65.54% Cd^{2+}, 94.93% Cu^{2+}, 97.64% Pb^{2+}, and 64.38% Zn^{2+} ions. Following 20 min, the clearance percentage for Pb^{2+} and Cu^{2+} ions remained almost constant, and no noticeable alteration in biosorption was observed.

Nevertheless, the absorption rate of Cd^{2+} and Zn^{2+} ions decreased after the initial 20 min, although it persisted until reaching a plateau at 200 min. The sluggish rate may be attributed to the mechanism of metal cation dispersal into the permeable structure of the biosorbent. The decline in removal effectiveness over time may also be attributed to biosorption occurring at active spots within a monolayer. Once a plateau phase (equilibrium state) was reached at 200 min, a relation of equilibrium between sorption and desorption procedures was detected. This offered repulsive forces and a drop in the HM adsorption after 200 min and was connected to the saturation of solid surfaces since the HM ions should be able to travel very long distances via the small-sized pores with very high concentrations. Thus, mass transfer between the solid and liquid phases is declining over time.

10.3389/frwa.2025.1612232

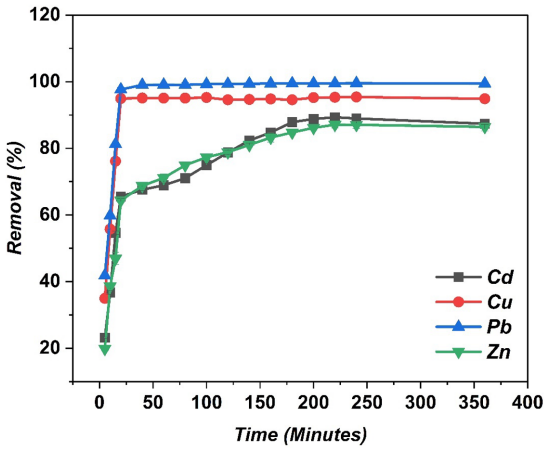

FIGURE 8
Impact of time (min) on the biosorption of Pb^{2+}, Cu^{2+}, Zn^{2+} andCd^{2+} via NSWR (pH = 5–6 ± 0.1, 0.01 M $NaNO_3$, stirring speed = 200 rpm, particle size = 250–90 μm, HMs solution volume = 50 ml, original HMs ions conc. = 50 mg/L (Cd^{2+}, Cu^{2+}, Pb^{2+}, Zn^{2+}), biosorbent mass = 0.5 ± 0.025 g).

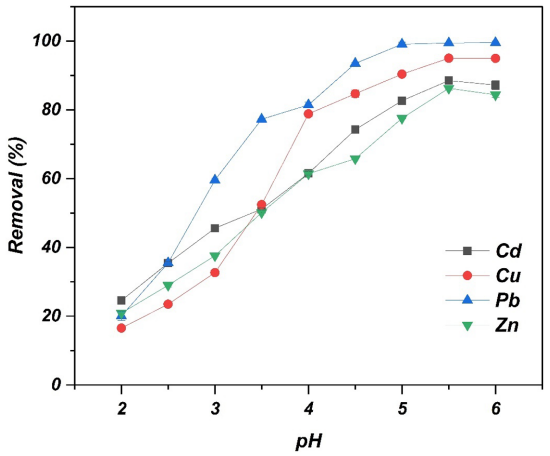

FIGURE 9
Impact of pH on the biosorption of Pb^{2+}, Cu^{2+}, Zn^{2+}, Cd^{2+} via NSWR, 0.01 M $NaNO_3$, stirring speed 200 rpm, particle size (250–90) μm, HMs solution volume = 50 ml, initial HMs ions conc. = 50 mg/L (Cd^{2+}, Cu^{2+}, Pb^{2+} and Zn^{2+}), biosorbent mass = 0.5 ± 0.025 g.

Notably, there was no significant improvement in biosorption for 4 ions after 200 min. Hence, a contact duration of 200 min was selected as the equilibrium time for subsequent studies. Nevertheless, it is important to note that time, as an influencing factor, is inadequate alone to give a full picture regarding the adsorption process, as the other parameters simultaneously and collectively affect the process in different ways and percentages.

3.3.3 Impact of pH

The absorption of HMs is significantly influenced by pH. It impacts the processes of hydrolysis, precipitation, dissociation, speciation, and accessibility of the HMs ions that collectively impact the biosorption procedure (Cruz-Lopes et al., 2021). Furthermore, the pH level is a crucial factor in the biosorption of HMs-ions as it influences the binding between the adsorbent and adsorbate compounds, as well as the charges of the functional groups on the biosorbent (Loh et al., 2020). In selecting the mechanism of metal removal (adsorption or precipitation), pH is paramount. The pH level decides both the surface charge and the chemical composition of the cell walls of the biosorbent. Indeed, it is crucial to initially adjust a solution's pH value before adjusting the other parameters.

This work aimed to examine the impact of pH on the biosorption of Pb^{2+}, Cu^{2+}, Zn^{2+}, and Cd^{2+} ions via NSWR at five different pH values: (2, 3, 4, 5, and 6). According to Figure 9, the percentages of Cd^{2+}, Cu^{2+}, Pb^{2+}, and Zn^{2+} cations absorbed by NSWR were seen to be low at pH 2 with values of 24.560, 16.533, 20.053, and 20.890, respectively. This phenomenon arises from the competition between HMs' cations and H^+ for the limited biosorption sites. Moreover, acidic conditions chemically facilitate the process of protonation of the functional groups on the NSWR, thereby producing repulsive interactions on the surface of the biosorbent and metal cations. Although the absorption percentage of the metals indicated above increased dramatically when the pH value went from 2 to 5, the specific scales of the upsurges were as follows: 52.28% for Cd^{2+}, 78.37% for Cu^{2+}, 79.017% for Pb^{2+}, and 56.65% for Zn^{2+}. This happening may be ascribed to the expanded presence of readily available negative charge surfaces on the adsorbent, which facilitated the capture of positively charged HMs cations. Furthermore, with an upsurge in pH, the adsorption surface exhibited a decline in positivity, resulting in an associated rise in electrostatic attraction between the HM ions and the NSWR surface. Within the pH range of 5–6, two relatively distinct behaviors were shown. For Cu^{2+} and Pb^{2+}, the enhancements in the uptake percentages were not significant, with values of only 0.817 and 0.2%. However, for Cd^{2+} and Zn^{2+}, the observed increases were 10.030 and 7.090%, respectively. The highest sorption effectiveness seen at pH 5.5–6 can be attributed to the interaction between Mi^+, $Mi(OH)^+$, and $Mi(OH)_2$, where Mi denotes the metal ions and surface functional groups that are present on (NSWR). This value, pH 5.5–6, corroborates the obtained magnitude of pH_{pzc} 5.7. The potential reduction in biosorption efficiency at higher pH levels (pH > 6) is not only due to the production of soluble hydroxylated complexes of HM ions (copper ions as $Cu(OH)_2$, cadmium ions as $Cd(OH)_2$, and lead ions as $Pb(OH)_2$) but also to the ionized state of the cell wall surface of the wood powder at the pH level under investigation (Munagapati et al., 2010). Hence, the experiment did not consider pH values above 6, as higher pH has been shown to induce precipitation of both Pb and Cu ions (Kariuki et al., 2017). The results of our study align with a review paper authored by Bhattacharjee and colleagues, which states that the ideal pH range for the absorption of HMs utilizing various cellulosic-based materials as biosorbents is mostly between 5 and 6 (Bhattacharjee et al., 2020).

3.3.4 Impact of temperature

The solution temperature is an influential operational cause that impacts the transport and kinetic mechanisms of HM ion adsorption. This characteristic is conditional on the mobility of HM ions and the swelling effect inside the inner structure of the biomaterials, which in turn impacts the adsorption capabilities.

In this study, the impact of temperature was examined within the temperature range of 25–45°C. It may be inferred that the impact of temperature on the proportion of deletion of 4 HM ions under

consideration was directly proportional to the uptake proportion. Specifically, as the temperature rose from 25 to 45°C, the elimination uptake also expanded. This observation suggests that the sorption process is endothermic. The observed rise can be recognized by the enhanced mobility of HM cations, which in turn leads to a rise in the number of active spots. The impact of temperature rise on the removal% % of the studied HMs is not remarkable. The same result was obtained from Tounsadi et al. (2015) using *Diplotaxis harra* and *Glebionis coronaria L.* biomasses for the removal of Cd (II) and Co (II) (Figure 10)

3.3.5 Impact of particle size

The primary factor responsible for physisorption is the intermolecular or electrostatic binding between HM ions and the adsorbent. This attraction could be strengthened by increasing the specific surface area of the adsorbent (Kumar et al., 2019). Though biosorption is a surface phenomenon that depends to some degree on the specific area unprotected from biosorption, only a limited number of studies have investigated the impact of altering the size of adsorbent particles on adsorption, especially in the case of non-living LCB.

The present work has demonstrated the impact of the particle size of NWSR on the ratio of uptake of the investigated HMs. The phenomenon was investigated in 5 distinct particle size classifications, as elucidated in Figure 11. Based on the flaky shape and relatively porous structure of NSWR particles, it can be inferred that they have acquired both an external and an internal surface that is readily accessible for the aqueous phase to penetrate, therefore facilitating the adsorption of HMs-ions to the active ligation adsorption sites (Božić et al., 2009). Importantly, the ratio at which 4 divalent cations (Cd^{2+}, Cu^{2+}, Pb^{2+}, and Zn^{2+}) are removed slightly increases when the particle size is reduced from 1,000 to 250 µm. Consequently, it may be inferred that a smaller particle size of the adsorbent results in a greater number of binding sites and a higher specific surface area, hence improving the effectiveness of removing bivalent hazardous metals. Meanwhile, fine particles also enhance the rapid adsorption rate and decrease the desired reaction time. As the particle size grows, the contact time required to achieve equilibrium also rises. Furthermore, the distance that the cations travel along the diffusion pathway across the bivalent cations of the sorbent is significantly reduced. In contrast, within the range of finer particles, specifically those smaller than 90 µm, the deletion percentages of Cd^{2+} and Cu^{2+} cations showed no increase, while the uptake rates of Cd^{2+} and Pb^{2+} cations somewhat decreased.

3.3.6 Impact of initial metal ion concentration

Multicomponent adsorption exhibits a lower removal effectiveness of manifold HM pollutants compared to the single HMs elimination efficacy achieved by a similar adsorbent. Furthermore, the inconsistency in the sequence of selectivity is attributed to variations in physicochemical characteristics, including electronegativity, hydrated radius, ionic radius, and covalent indexes (Table 5). This behavior may also be attributed to the polarizability of HM ions and, to a certain degree, to the hard-soft acid–base (HSAB) theory: typically, hard acids exhibit stronger coordination with hard bases and soft acids with soft bases (Bulin et al., 2022). The adsorption efficiency of NSWR for HMs ions in water can be affected by several factors, including the type and quantity of functional groups, specific surface area, surface shape, and structural features. Our results demonstrate a selective adsorption pattern, with Pb having the greatest adsorption capacity, followed by Cu, then Cd. Finally, Zn is shown in Figure 12. A recent review article by Amar et al. (2021) has concluded that throughout modest biosorption from multi-metal systems, most biosorbents can efficiently eliminate Pb^{2+} even when other HMs are exhibited. Nonetheless, the incidence of Pb^{2+} ions significantly lowered the adsorption of Cu^{2+}, Cd^{2+}, Zn^{2+}, Ni^{2+}, and Cr^{3+}. Investigation of the adsorption of HM ions in a quaternary system utilizing *Kappaphycus* sp. illustrates the adsorption ranking of Pb^{2+}, Cu^{2+}, Fe^{2+}, and Zn^{2+} as reported by Natrayan et al. (2022). Furthermore, when Pine bark was applied, the order observed was $Pb^{2+} > Cu^{2+} > Fe^{2+} > Zn^{2+}$ (Cutillas-Barreiro et al., 2014). Similarly,

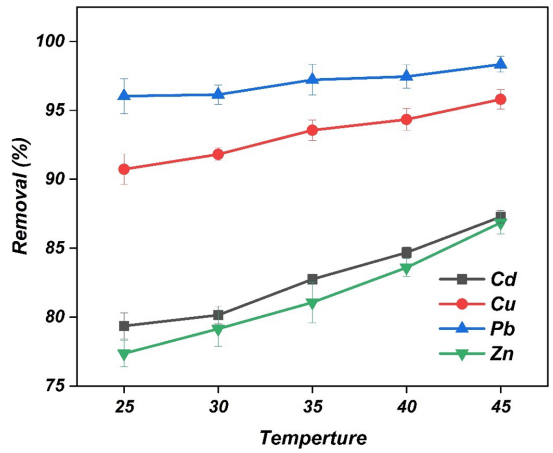

FIGURE 10
Impact of temperature (°C) on the biosorption of Cd^{2+}, Cu^{2+}, Pb^{2+}, and Zn^{2+} via NSWR. pH = 5–6 ± 0.1, stirring speed = 200 rpm, 0.01 M $NaNO_3$, particle Size = (250–90) µm, HMs solution volume = 25 ml, initial HMs ions conc. = 50 mg/L (Cd^{2+}, Cu^{2+}, Pb^{2+} and Zn^{2+}, biosorbent mass = 0.5 ± 0.025 g.

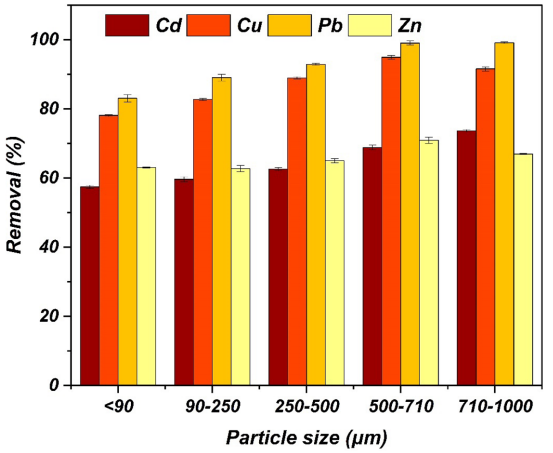

FIGURE 11
Impact of particle size (µm) on the biosorption of Cd^{2+}, Cu^{2+}, Pb^{2+}, and Zn^{2+} via NSWR. pH = 5–6 ± 0.1, stirring speed = 200 rpm,0.01 M $NaNO_3$, HMs solution volume = 50 ml, initial HMs ions conc. = 50 mg/L (Cd^{2+}, Cu^{2+}, Pb^{2+} and Zn^{2+}), biosorbent mass = 0.5 ± 0.025 g.

10.3389/frwa.2025.1612232

TABLE 5 Physiochemical features of the HMs ions utilized herein.

Elements	Cd	Cu	Pb	Zn
C.F	$CdCl_2.2.5H_2O$	$Cu(NO_3)_2.3H_2O$	$Pb(NO_3)_2$	$Pb(NO_3)_2$
M.M	112.41	63.546	207.2	65.38
G	IIB	IB	IVA	IIB
A.R	1.48	1.35	1.54	1.31
E	1.69	1.9	2.33	1.65
H.R	4.26	4.19	4.01	4.30
C.I	2.71	2.98	6.41	2.04
A.N	48	29	82	30
H.E	−1807	−2,100	−1,481	−2046
I.R	0.97	0.72	1.33	0.74
E.C	[Kr] $4d^{10}5s^2$	[Ar] $3d^{10}4s^1$	[Xe] $6s^2$ $4f^{14}$ $5d^{10}$ $6p^2$	[Ar] $3d^{10}4s^2$

**A.R: Atomic Radius (Å), E: Electronegativity, C.F: Chemical Formula, H.R: Hydrated Radius (Å), M.M: Mole Mass (g/mol), A.N: Atomic Number, G: Group, H.E: Hydration Energy KJ/mol, E.C: Electron Configuration, I.R: Ionic Radius (Å), C.I: Covalent Index. Sources: Kong et al., 2020; Wang et al., 2021; Fertu et al., 2022.

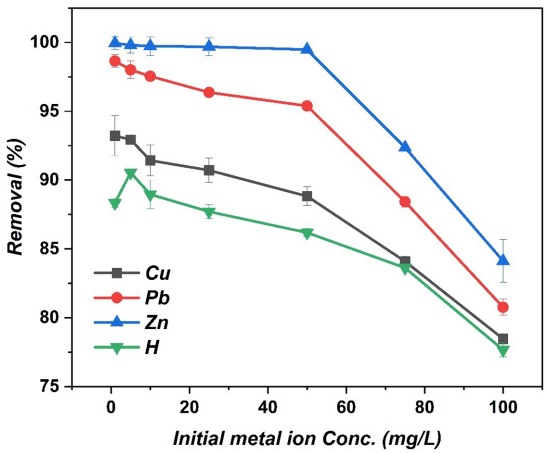

FIGURE 12
Impact of initial metal ion concentration (mg/L) on the biosorption of Cd^{2+}, Cu^{2+}, Pb^{2+} and Zn^{2+} via NSWR. PH = 5–6 ± 0.1, 0.01 M $NaNO_3$, temperature = 25.4°C ± 0.3°C, stirring speed = 200 rpm, particle size = (250–90) µm, HMs solution volume 50 ml, initial HMs ions conc. = 50 mg/L (Cd^{2+}, Cu^{2+}, Pb^{2+} and Zn^{2+}),biosorbent mass = 0.5 ± 0.025 g.

Anastopoulos et al. (2019) reported $Pb^{2+} > Cu^{2+} > Zn^{2+}$ arrangement on watermelon rinds. A metal ion's covalent index is determined by its ionic radius and electronegativity. A higher covalent index indicates a better potential for the metal ion to form covalent bonds with the functional groups of the biosorbent (Batool et al., 2022). The covalent index of Pb is 6.41, while Cu, Cd, and Zn have covalent index values of 2.98, 2.71, and 2.04, respectively. Furthermore, the level of toxicity often rises as the covalent index magnitude increases. The data presented in Table 5

TABLE 6 (LC) adsorbents used in literature for HMs removal and their q_{max} values.

Maximum Adsorption Capacity,q_{max} (mg/g)	Element	Adsorbent	Source
11,4.9	Cu^{2+}, Zn^{2+}	Teakwood SDT	Shukla and Pai (2005)
6.35,2.87	Pb^{2+}, Cd^{2+}	*Picea smithiana* SDT*	Mahmood-ul-Hassan et al. (2018)
4.54, 4.32	Zn^{2+}, Cu^{2+}	*Carpinus betulus*	Zolgharnein et al. (2017)
10.125,8.48, 8.87	Pb^{2+}, Zn^{2+}, Cd^{2+}	*Populus alba* SDT	Najam and Andrabi (2016)
3.96, 4.4	Cu^{2+}, Zn^{2+}	Hornbeam SDT	Kovacova et al. (2020)
2.16, 1.46	Cu^{2+}, Zn^{2+}	Cherry SDT	
3.88, 2.88	Cu^{2+}, Zn^{2+}	Poplar SDT	
2.48, 2.01	Cu^{2+}, Zn^{2+}	Spruce SDT (raw)	
81.87, 117.3	Pb^{2+}, Cd^{2+}	Cypress Fruit- AC	Al-Ma'abreh et al. (2024a)
85.22, 75.34	Pb^{2+}, Cd^{2+}	Cypress-AC	Al-Ma'abreh et al. (2024b)
98.15, 89.21	Pb^{2+}, Cu^{2+}	Oak Cupules-AC	Khater et al. (2024)
6.3, 7.9, 10.3, 6.0	Cd^{2+}, Cu^{2+}, Pb^{2+}, Zn^{2+}	*Picea abies* (L.) Karst	This study

*SDT: sawdust.

demonstrates a positive correlation between electronegativity, covalent index, and ion exchange. Consequently, the sorption capacity also increases. These results align with the works of Baool and coworkers (Batool et al., 2022). The adsorption kinetics of HMs-cations on particle surfaces, particularly in multi-ion solutions, are intricate and cannot be fully elucidated only based on electrostatic or ion-exchange adsorption, cation size, or hydration. It is necessary to consider all possible mechanisms comprehensively and succinctly. Overall, the variability in the sequence of selectivity can be associated with variations in physicochemical characteristics, including electronegativity, hydrated radius, ionic radius, and covalent indexes, and can be potentially connected to the "shielding effect" or "screening effect" of HM cations (Table 5). Furthermore, (Table 6) lists several types of biomass together with their related q_{max} values. Among these, unmodified NSWR is a highly favorable material for bio-sequestration when compared to other lean bio-adsorbents.

3.3.7 Impact of agitation speed

The speed of agitation is a salient aspect in biosorption investigations, particularly in the context of porous materials such as LCB. However, scholars have not adequately taken it into account. Indeed, effective agitation potentially promotes the infiltration of HM ions into the internal framework of the biosorbent, accelerates the mobility of HM ions in the solutions

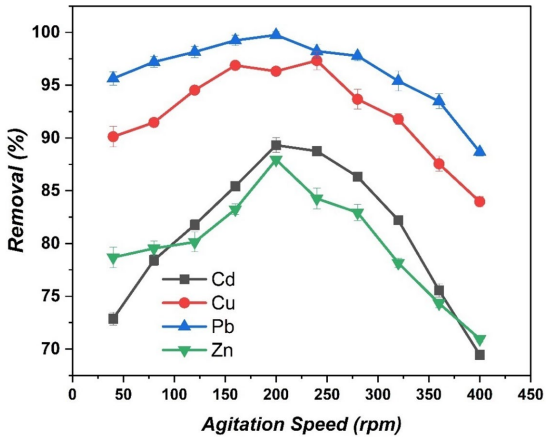

FIGURE 13
Impact of stirring speed (rpm) on the biosorption of Cd^{2+}, Cu^{2+}, Pb^{2+} and Zn^{2+} via NSWR. pH = 5–6 ± 0.1, 0.01 M $NaNO_3$, Particle Size = (250–90) µm, HMs solution volume = 70 ml, Initial HMs ions conc. = 50 mg/L (Cd^{2+}, Cu^{2+}, $Pb^{2+}$and Zn^{2+}, biosorbent mass = 0.5 ± 0.025 g.

containing the metal, decreases the duration of the reaction, and optimizes the transfer of mass resistance, thereby improving the biosorption process.

To investigate the impact of agitation speed on HM bio-absorption, we examined 10 distinct mixing speeds ranging from 40 to 400 rpm, as detailed in Figure 13. At agitation speeds below 150 rpm, the elimination uptake was quite low. It is probable that a portion of the adsorbent settled down and did not participate in adsorption, resulting in a reduction in biosorption. As the agitation speed increases within 150–200 rpm, the turbulence in the liquid phase intensifies, leading to higher external mass transfer coefficients and decreased boundary layer effect. Thus, the decrease in external resistance results in accelerated adsorption (Sreedhar and Reddy, 2019). On the other hand, whenever the stirring speed exceeds 200 rpm, the adsorbent may not have sufficient time to bind the HM cations, therefore decreasing its effectiveness. It is vital to note that the shaking ratio should be appropriate and adequate to guarantee the easy availability of all surface binding spots for the absorption of HM ions. The results of this study have demonstrated that an agitation speed of around 200 rpm is sufficient and appropriate for the absorption of the four ions under investigation. Similar outcomes were achieved when *Moringa stenopetala* bark was used for the removal of Cd^{2+}, Pb^{2+}, and Cu^{2+} (Kebede et al., 2018).

3.4 Adsorption isotherm study

To elucidate the equilibrium characteristics of heavy metal adsorption onto NSWR and understand the interactions between the adsorbate (HM ions) and the adsorbent surface, the experimental equilibrium data were analyzed using the Langmuir and the Freundlich isotherm models. These models provide insights into the adsorption capacity, surface properties (homogeneous vs. heterogeneous), and the affinity between the sorbent and sorbate. The linear or non-linear fits of the Langmuir and Freundlich models to the experimental data for Cd^{2+}, Cu^{2+}, Pb^{2+}, and Zn^{2+} adsorption is presented in Figure 14. The calculated isotherm parameters, including maximum adsorption capacities, affinity constants, and correlation coefficients (R^2), derived from these fits, are summarized in Table 6. A comparison of the correlation coefficients (R^2) indicates that the Langmuir model provides a superior fit to the experimental data for all four HMs ($R^2 \approx 0.99$) compared to the Freundlich model ($R^2 \approx 0.90$–0.96). This suggests that the adsorption process onto NSWR aligns well with the assumptions of the Langmuir isotherm: predominantly monolayer adsorption occurring on a finite number of identical and energetically equivalent active sites on the biosorbent surface, with no interaction between adsorbed molecules (Akpomie et al., 2023; Mo et al., 2023). This type of fit often points toward chemisorption playing a significant role in the binding process. The maximum monolayer adsorption capacities (q_m) estimated from the Langmuir model (Table 7) followed the order: Pb^{2+} (10.325 mg/g) > Cu^{2+} (7.853 mg/g) > Cd^{2+} (6.277 mg/g) > Zn^{2+} (6.029 mg/g). These values represent the theoretical saturation capacity of the NSWR under the applied experimental conditions.

Although the Freundlich model provided a less accurate fit, its parameters offer complementary information. The Freundlich constant K_f relates to adsorption capacity, while the intensity factor 1/n indicates the favorability and degree of surface heterogeneity. The obtained 1/n values were all less than 1 (ranging from 0.55 to 0.675, Table 7), which also signifies favorable adsorption. Values of $1/n < 1$ typically suggest chemisorption processes or some degree of surface heterogeneity, which might coexist even if the overall process is best approximated by the Langmuir model.

4 Conclusion

This study successfully demonstrated the viability of utilizing unmodified (NSWR), an abundant and cost-effective biomass, as a biosorbent for the simultaneous removal of Pb^{2+}, Cu^{2+}, Cd^{2+}, and Zn^{2+} ions from multi-component aqueous solutions. The investigation confirmed that various operational parameters influence NSWR's adsorption performance. Optimal conditions for removal were identified, including a contact time reaching equilibrium around 200 min (with over 60% removal occurring rapidly within the first 20 min), an initial heavy metal concentration range where adsorption capacity increased accordingly, an effective pH range of 5.0–6.0, moderately elevated temperatures (suggesting an endothermic process within the 25–45°C range), and finer particle sizes (specifically 90–250 µm). Key factors significantly impacting the process were solution pH, adsorbent dosage, and initial metal ion concentration. The adsorption process was effectively described by the Langmuir isotherm model, indicating favorable monolayer adsorption onto a relatively homogeneous surface, with maximum capacities determined as 10.3, 7.9, 6.3, and 6.0 mg/g for Pb^{2+}, Cu^{2+}, Cd^{2+}, and Zn^{2+}, respectively. The underlying mechanisms likely involve a combination of processes, including ion exchange, supported by the presence of inherent cations like Ca^{2+} (confirmed via EDS), and surface complexation/chelation involving oxygen-containing functional groups (identified by FTIR). Electrostatic interactions

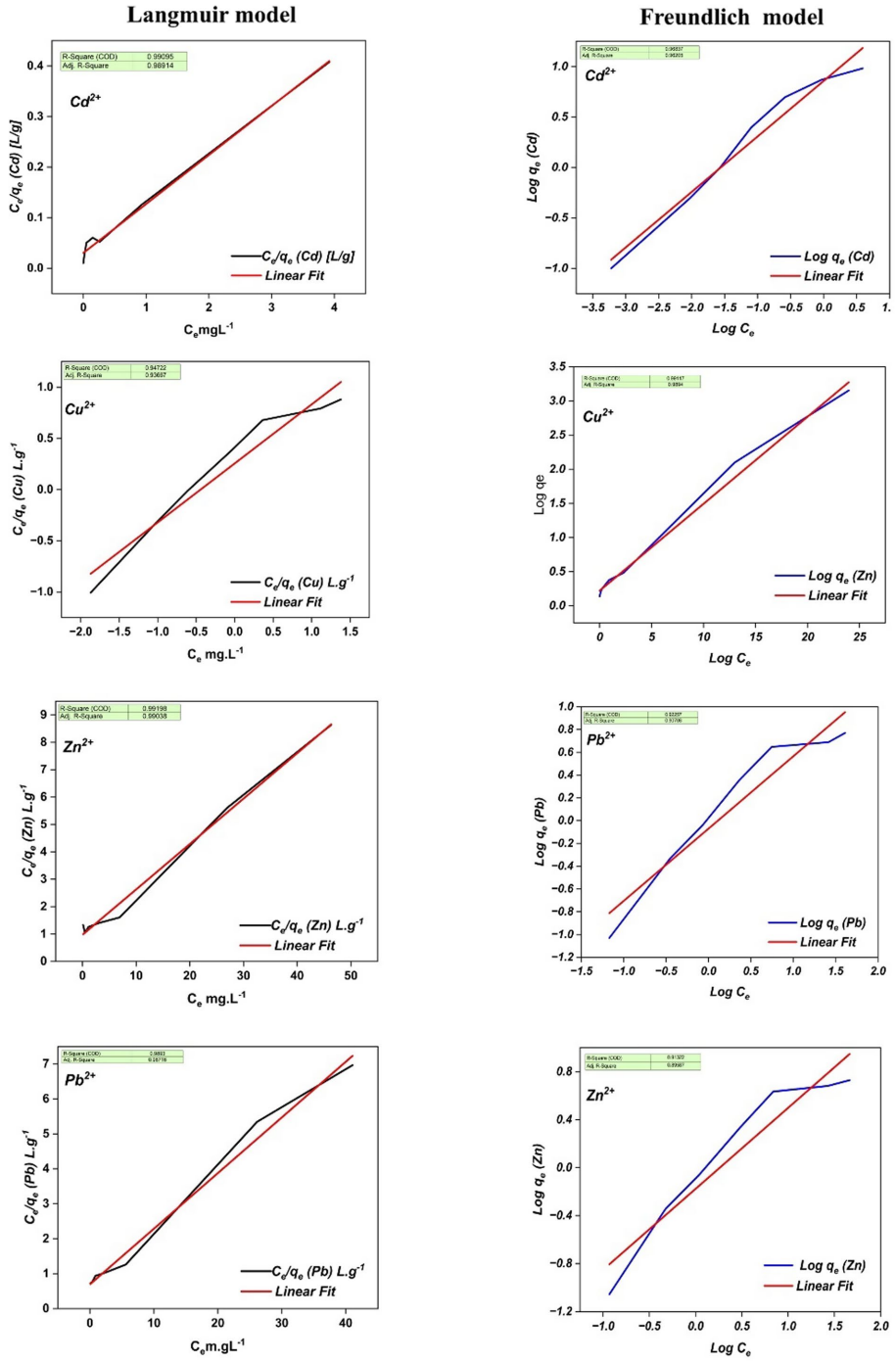

FIGURE 14
Linearized plots of the Langmuir (C_e/q_e vs. C_e) and Freundlich (Log q_e vs. Log C_e) isotherm models fitted to the experimental equilibrium adsorption data for Cd^{2+}, Cu^{2+}, Pb^{2+}, and Zn^{2+} onto (NSWR).

also play a role governed mainly by the solution pH relative to the NSWR's pH_{pzc} of 5.7. The predominantly amorphous nature of the NSWR, confirmed by XRD, likely facilitates accessibility to these binding sites. In addition, NSWR showed good thermal stability.

The observed preferential adsorption followed the sequence $Pb^{2+} > Cu^{2+} > Cd^{2+} > Zn^{2+}$, correlating well with the physicochemical properties of the ions, such as their covalent index, which influences their affinity for the biosorbent's active sites.

In conclusion, unmodified NSWR emerges as a promising, sustainable, and readily available biosorbent for treating water contaminated with multiple HMs. This study highlights a valuable "trash-to-treasure" approach, offering an effective means for WW detoxification while simultaneously providing productive use for bio-industrial waste, thereby reducing potential environmental accumulation. The effectiveness demonstrated in a multi-metal system underscores its potential relevance for real-world applications.

TABLE 7 Isotherm parameters for Pb^{2+}, Cd^{2+}, Cu^{2+}, and Zn^{2+} biosorption, using NSWR as biosorbent.

Element	Model
	Langmuir
Cd^{2+}	q_m(mg/g) = 6.277, K_L (Lm/g) = 0.2298, $R^2 \approx 99$
Pb^{2+}	q_m(mg/g) = 10.325, K_L (L/mg) = 3.211, $R^2 \approx 0.99$
Cu^{2+}	q_m(mg/g) = 7.853, K_L (L/mg) = 0.5785, $R^2 \approx 0.99$
Zn^{2+}	q_m(mg/g) = 6.029, K_L (L/mg) = 0.1712, $R^2 \approx 0.99$
	Freundlich
Cd^{2+}	K_f (mg/g) = 0.9312, 1/n (g/L) = 0.635, $R^2 \approx 0.91$
Pb^{2+}	K_f (mg/g) = 2.3577, 1/n (g/L) = 0.55, $R^2 \approx 0.96$
Cu^{2+}	K_f (mg/g) = 1.2915, 1/n = 0.576, $R^2 \approx 0.94$
Zn^{2+}	K_f (mg/g) = 0.8383, 1/n (g/L^1) = 0.675, $R^2 \approx 0.9$

Data availability statement

The datasets presented in this study can be found in online repositories. The names of the repository/repositories and accession number(s) can be found in the article/supplementary material.

Author contributions

IA-L: Formal analysis, Writing – review & editing, Writing – original draft, Data curation, Investigation, Conceptualization. MH: Writing – original draft, Supervision, Formal analysis, Writing – review & editing, Data curation, Conceptualization. AA: Writing – review & editing, Software, Visualization, Data curation. AA-M: Writing – review & editing, Writing – original draft, Software, Methodology. MB: Writing – review & editing, Data curation, Software, Validation, Visualization. BK: Writing – review & editing, Visualization, Software, Validation, Methodology. GH: Data curation, Writing – review & editing, Software, Visualization. WA: Writing – review & editing, Resources, Funding acquisition, Validation, Project administration. MA: Visualization, Software, Writing – review & editing, Conceptualization. HA: Methodology, Software, Resources, Project administration, Writing – review & editing. ME: Methodology, Software, Writing – review & editing.

Funding

The author(s) declare that financial support was received for the research and/or publication of this article. The authors are incredibly grateful for the "Stipendium Hungaricum Scholarship" funding. The authors acknowledge Princess Nourah bint Abdulrahman University Researchers Supporting Project number (PNURSP2025R458), Princess Nourah bint Abdulrahman University, Riyadh, Saudi Arabia. The Flagship Research Groups Program of the Hungarian University of Agriculture and Life Sciences also funded it.

Conflict of interest

The authors declare that the research was conducted in the absence of any commercial or financial relationships that could be construed as a potential conflict of interest.

Generative AI statement

The author(s) declare that no Gen AI was used in the creation of this manuscript.

Publisher's note

All claims expressed in this article are solely those of the authors and do not necessarily represent those of their affiliated organizations, or those of the publisher, the editors and the reviewers. Any product that may be evaluated in this article, or claim that may be made by its manufacturer, is not guaranteed or endorsed by the publisher.

References

Abdulkareem, A. S., Hamzat, W. A., Tijani, J. O., Egbosiuba, T. C., Mustapha, S., Abubakre, O. K., et al. (2023). Isotherm, kinetics, thermodynamics and mechanism of metal ions adsorption from electroplating wastewater using treated and functionalized carbon nanotubes. *J. Environ. Chem. Eng.* 11:109180. doi: 10.1016/j.jece.2022.109180

Abi Bianasari, A., Khaled, M. S., Hoang, T.-D., Reza, M. S., Bakar, M. S. A., and Azad, A. K. (2024). Influence of combined catalysts on the catalytic pyrolysis process of biomass: a systematic literature review. *Energy Convers. Manag.* 309:118437. doi: 10.1016/j.enconman.2024.118437

Abou-Elyazed, A. S., Shaban, A. K. F., Osman, A. I., Heikal, L. A., Mohamed, H. F. M., Hassan, W. M. I., et al. (2024). Comparative catalytic efficacy of cost-effective MIL-101(Cr) based PET waste for biodiesel production. *Curr. Res. Green Sustain. Chem.* 8:100401. doi: 10.1016/j.crgsc.2024.100401

Akpomie, K. G., Conradie, J., Adegoke, K. A., Oyedotun, K. O., Ighalo, J. O., Amaku, J. F., et al. (2023). Adsorption mechanism and modeling of radionuclides and heavy metals onto ZnO nanoparticles: a review. *Appl Water Sci* 13:20. doi: 10.1007/s13201-022-01827-9

Ali, Z., Ullah, R., Tuzen, M., Ullah, S., Rahim, A., and Saleh, T. A. (2023). Colorimetric sensing of heavy metals on metal doped metal oxide nanocomposites: a review. *Trends Environ. Anal. Chem.* 37:e00187. doi: 10.1016/j.teac.2022.e00187

Al-Labadi, I. G., Shemy, M. H., Ghidan, A. Y., Allam, A. A., Kálmán, H. M., Ajarem, J. S., et al. (2023). Insight into the effects of H2SO4 and HNO3 acidification processes on the properties of coal as an enhanced adsorbent for ciprofloxacin residuals: steric and energetic studies. *Front. Chem.* 11:1130682. doi: 10.3389/fchem.2023.1130682

Al-Ma'abreh, A. M., AlKhabbas, M., Alawaideh, S., Hussein-Al-Ali, S. H., Hmedat, D. A., Edris, G., et al. (2024a). Investigation of kinetics, thermodynamics, and isotherms of the simultaneous removal of heavy metal ions by activated carbon from cypress fruit. *Adsorpt. Sci. Technol.* 42 02636174241256853:02636174241256853. doi: 10.1177/02636174241256853

Al-Ma'abreh, A. M., Hmedat, D. A., Edris, G., and Hamed, M. A. (2024b). Removal of heavy metal ions (Pb2+, Co2+, and Cd2+) by activated carbon from cypress fruit: an investigation of kinetics, thermodynamics, and isotherms. *J. Chem.* 2024:1984821. doi: 10.1155/2024/1984821

Al-Mur, B. A. (2024). Application of marine mollusk shells (meretrix lusoria) as low-cost biosorbent for removing cd2+ and pb2+ ions from aqueous solution: kinetic and equilibrium study. *Water.* 16:2615.

Amar, M. B., Walha, K., and Salvadó, V. (2021). Valorisation of pine cone as an efficient biosorbent for the removal of Pb (II), Cd (II), Cu (II), and Cr (VI). *Adsorpt. Sci. Technol.* 2021, 1–12. doi: 10.1155/2021/6678530

Anastopoulos, I., Robalds, A., Tran, H. N., Mitrogiannis, D., Giannakoudakis, D. A., Hosseini-Bandegharaei, A., et al. (2019). Removal of heavy metals by leaves-derived biosorbents. *Environ. Chem. Lett.* 17, 755–766. doi: 10.1007/s10311-018-00829-x

Armaya'u, U., Zango, M. U., Ariffin, M. M., Khalik, W. M. A. W. M., Yusoff, H. M., Zango, Z. U., et al. (2024). Copper(II) isonicotinate metal-organic framework for reusable adsorption of salmeterol from wastewater. *Sustain. Chem. One World* 4:100030. doi: 10.1016/j.scowo.2024.100030

Awan, K. M., Yu, H., Wang, L., Basit, A., Keshta, B. E., Wang, Y., et al. (2024). Microneedles for anti-aging skincare: preparation, properties and applications. *Mater. Today Commun.* 41:110740. doi: 10.1016/j.mtcomm.2024.110740

Basit, A., Yu, H., Wang, L., Uddin, M. A., Wang, Y., Awan, K. M., et al. (2024). Recent advances in wet surface tissue adhesive hydrogels for wound treatment. *Eur. Polym. J.* 216:113260. doi: 10.1016/j.eurpolymj.2024.113260

Batool, F., Irfan, A., Al-Hussain, S. A., Al-Farraj, E. S., Iqbal, S., Akbar, J., et al. (2022). Development of ion character property relationship (IC-PR) for removal of 13-metal ions by employing a novel green adsorbent *Aerva javanica*. *Molecules* 27:8213. doi: 10.3390/molecules27238213

Bhardwaj, A., Bansal, M., Wilson, K., Gupta, S., and Dhanawat, M. (2025). Lignocellulose biosorbents: unlocking the potential for sustainable environmental cleanup. *Int. J. Biol. Macromol.*:139497. doi: 10.1016/j.ijbiomac.2025.139497

Bhattacharjee, C., Dutta, S., and Saxena, V. K. (2020). A review on biosorptive removal of dyes and heavy metals from wastewater using watermelon rind as biosorbent. *Environ. Adv.* 2:100007. doi: 10.1016/j.envadv.2020.100007

Božić, D., Stanković, V., Gorgievski, M., Bogdanović, G., and Kovačević, R. (2009). Adsorption of heavy metal ions by sawdust of deciduous trees. *J. Hazard. Mater.* 171, 684–692. doi: 10.1016/j.jhazmat.2009.06.055

Bulin, C., Zheng, R., Guo, T., and Zhang, B. (2022). Incorporating hard-soft acid-base theory in multi-aspect analysis of the adsorption mechanism of aqueous heavy metals by graphene oxide. *J. Phys. Chem. Solids* 170:110934. doi: 10.1016/j.jpcs.2022.110934

Chen, H., He, Y., Han, Y., Hu, J., Li, J., Jiang, Y., et al. (2025). A new SIFSIX anion pillared cage MOF with crs topological structure for efficient C2H2/CO2 separation. *Chin. J. Struct. Chem.* 44:100508. doi: 10.1016/j.cjsc.2024.100508

Chen, X., Zhao, B., Shuai, C., Qu, S., and Xu, M. (2022). Global spread of water scarcity risk through trade. *Resour. Conserv. Recycl.* 187:106643. doi: 10.1016/j.resconrec.2022.106643

Cruz-Lopes, L. P., Macena, M., Esteves, B., and Guiné, R. P. F. (2021). Ideal pH for the adsorption of metal ions Cr6+, Ni2+, Pb2+ in aqueous solution with different adsorbent materials. *Open Agric.* 6, 115–123. doi: 10.1515/opag-2021-0225

Cutillas-Barreiro, L., Ansias-Manso, L., Fernández-Calviño, D., Arias-Estévez, M., Nóvoa-Muñoz, J. C., Fernández-Sanjurjo, M. J., et al. (2014). Pine bark as bio-adsorbent for Cd, Cu, Ni, Pb and Zn: batch-type and stirred flow chamber experiments. *J. Environ. Manag.* 144, 258–264. doi: 10.1016/j.jenvman.2014.06.008

Deka, B. K., and Maji, T. K. (2013). Effect of SiO2 and nanoclay on the properties of wood polymer nanocomposite. *Polym. Bull.* 70, 403–417. doi: 10.1007/s00289-012-0799-6

Demirbas, A. (2008). Heavy metal adsorption onto agro-based waste materials: a review. *J. Hazard. Mater.* 157, 220–229. doi: 10.1016/j.jhazmat.2008.01.024

Ezzeddine, Z., Batonneau-Gener, I., Ghssein, G., and Pouilloux, Y. (2025). Recent advances in heavy metal adsorption via organically modified mesoporous silica: a review. *Water (Basel)* 17:669. doi: 10.3390/w17050669

Fertu, D. I., Bulgariu, L., and Gavrilescu, M. (2022). Modeling and optimization of heavy metals biosorption by low-cost sorbents using response surface methodology. *PRO* 10:523. doi: 10.3390/pr10030523

Freundlich, H. M. F. (1906). Over the adsorption in solution. *J. Phys. Chem.* 57, 1100–1107.

Hao, Z., Qian, J., Zheng, F., Lin, B., Xu, M., Feng, W., et al. (2024). Human-influenced changes in pollution status and potential risk of sediment heavy metals in Xincun Bay, a typical lagoon of Hainan, China. *Mar. Pollut. Bull.* 199:115949. doi: 10.1016/j.marpolbul.2023.115949

Hiew, B. Y. Z., Lee, L. Y., Lee, X. J., Thangalazhy-Gopakumar, S., and Gan, S. (2021). Utilisation of environmentally friendly okara-based biosorbent for cadmium (II) removal. *Environ. Sci. Pollut. Res.* 28, 40608–40622. doi: 10.1007/s11356-020-09594-3

Hoang, T., Van Anh, N., Yusuf, M., Ali, S. A. M., Subramanian, Y., Hoang Nam, N., et al. (2024). Valorization of agriculture residues into value-added products: a comprehensive review of recent studies. *Chem. Rec.* 24:e202300333. doi: 10.1002/tcr.202300333

Hussain, M., Ali, A. S., Kousar, T., Mahmood, F., Haruna, A., Zango, Z. U., et al. (2025). Efficient removal of manganese (II) ions from aqueous solution using biosorbent derived from rice husk. *Sustain. Chem. One World* 5:100047. doi: 10.1016/j.scowo.2025.100047

Ivanovska, A., Veljović, S., Dojčinović, B., Tadić, N., Mihajlovski, K., Natić, M., et al. (2021). A strategy to revalue a wood waste for simultaneous cadmium removal and wastewater disinfection. *Adsorpt. Sci. Technol.* 2021:3552300. doi: 10.1155/2021/3552300

Javeria, H., Abbas, M. Q., Chen, S.-H., Keshat, B. E., and Du, Z. (2025). Scalability of sulfur-functionalized carbon quantum dots from peanut shells: a sustainable sensor of high colorimetric heavy metal detection. *J. Environ. Chem. Eng.* 13:115821. doi: 10.1016/j.jece.2025.115821

Jiang, J., Shi, Y., Ma, N. L., Ye, H., Verma, M., Ng, H. S., et al. (2024). Utilizing adsorption of wood and its derivatives as an emerging strategy for the treatment of heavy metal-contaminated wastewater. *Environ. Pollut.* 340:122830. doi: 10.1016/j.envpol.2023.122830

Kainth, S., Sharma, P., and Pandey, O. P. (2024). Green sorbents from agricultural wastes: a review of sustainable adsorption materials. *Appl. Surf. Sci. Adv.* 19:100562. doi: 10.1016/j.apsadv.2023.100562

Kariuki, Z., Kiptoo, J., and Onyancha, D. (2017). Biosorption studies of lead and copper using rogers mushroom biomass 'Lepiota hystrix'. *S. Afr. J. Chem. Eng.* 23, 62–70. doi: 10.1016/j.sajce.2017.02.001

Kebede, T. G., Dube, S., Mengistie, A. A., Nkambule, T. T. I., and Nindi, M. M. (2018). *Moringa stenopetala* bark: a novel green adsorbent for the removal of metal ions from industrial effluents. *Phys. Chem. Earth. Part A/B/C* 107, 45–57. doi: 10.1016/j.pce.2018.08.002

Keshta, B. E., Yu, H., and Wang, L. (2023). MIL series-based MOFs as effective adsorbents for removing hazardous organic pollutants from water. *Sep. Purif. Technol.* 322:124301. doi: 10.1016/j.seppur.2023.124301

Keshta, B. E., Yu, H., Wang, L., Uddin, M. A., El-Attar, H. G., Keshta, A. E., et al. (2024). Cost-effective synthesis of MIL-101(Cr) from recyclable wastes and composite with polyaniline as an ion-to-electron transducer for potentiometric Pb2+ sensing. *Chem. Eng. J.* 485:150049. doi: 10.1016/j.cej.2024.150049

Khater, D., Alkhabbas, M., and Al-Ma'abreh, A. M. (2024). Adsorption of Pb, Cu, and Ni ions on activated carbon prepared from oak cupules: kinetics and thermodynamics studies. *Molecules* 29:2489. doi: 10.3390/molecules29112489

Khedulkar, A. P., Bobade, R. G., Doong, R., Pandit, B., Ky, N. M., Ambare, R. C., et al. (2025). Bio-based nanomaterials as effective, friendly solutions and their applications for protecting water, soil, and air. *Mater Today Chem* 46:102688. doi: 10.1016/j.mtchem.2025.102688

Kong, Q., Preis, S., Li, L., Luo, P., Wei, C., Li, Z., et al. (2020). Relations between metal ion characteristics and adsorption performance of graphene oxide: a comprehensive experimental and theoretical study. *Sep. Purif. Technol.* 232:115956. doi: 10.1016/j.seppur.2019.115956

Kosmulski, M. (2023). The pH dependent surface charging and points of zero charge. X. Update. *Adv. Colloid Interf. Sci.* 319:102973. doi: 10.1016/j.cis.2023.102973

Kothavale, V. P., Sharma, A., Dhavale, R. P., Chavan, V. D., Shingte, S. R., Selyshchev, O., et al. (2023). Carboxyl and thiol-functionalized magnetic nanoadsorbents for efficient and simultaneous removal of Pb (II), Cd (II), and Ni (II) heavy metal ions from aqueous solutions: studies of adsorption, kinetics, and isotherms. *J. Phys. Chem. Solids* 172:111089. doi: 10.1016/j.jpcs.2022.111089

Kovacova, Z., Demcak, S., Balintova, M., Pla, C., and Zinicovscaia, I. (2020). Influence of wooden sawdust treatments on Cu (II) and Zn (II) removal from water. *Materials* 13:3575. doi: 10.3390/ma13163575

Kumar, P. S., Korving, L., Keesman, K. J., van Loosdrecht, M. C. M., and Witkamp, G.-J. (2019). Effect of pore size distribution and particle size of porous metal oxides on phosphate adsorption capacity and kinetics. *Chem. Eng. J.* 358, 160–169. doi: 10.1016/j.cej.2018.09.202

Langmuir, I. (1918). The adsorption of gases on plane surfaces of glass, mica and platinum. *J. Am. Chem. Soc.* 40, 1361–1403. doi: 10.1021/ja02242a004

Liu, L., Gao, Z. Y., Su, X. P., Chen, X., Jiang, L., and Yao, J. M. (2015). Adsorption removal of dyes from single and binary solutions using a cellulose-based bioadsorbent. *ACS Sustain. Chem. Eng.* 3, 432–442. doi: 10.1021/sc500848m

Loh, J. Y., Khor, A. H.-Y., Lai, K. S., and Liew, H. J. (2020). Biosorption efficacy of alginate-immobilized live and metal chloride-activated *Azolla microphylla* in Pb (II) removal from aqueous solution. *Int. Aquat. Res.* 12. doi: 10.26872/jmes.2018.9.1.23

Mahmood-ul-Hassan, M., Yasin, M., Yousra, M., Ahmad, R., and Sarwar, S. (2018). Kinetics, isotherms, and thermodynamic studies of lead, chromium, and cadmium bio-adsorption from aqueous solution onto *Picea smithiana* sawdust. *Environ. Sci. Pollut. Res.* 25, 12570–12578. doi: 10.1007/s11356-018-1300-3

Marin, J., and Ayele, J. (2002). Removal of some heavy metal cations from aqueous solutions by spruce sawdust. I. Study of the binding mechanism through batch experiments. *Environ. Technol.* 23, 1157–1171. doi: 10.1080/09593332308618334

Mathew, B. B., Jaishankar, M., Biju, V. G., and Beeregowda, K. N. (2016). Role of bioadsorbents in reducing toxic metals. *J. Toxicol.* 2016, 1–13. doi: 10.1155/2016/4369604

Matin, B., Brandić, I., Matin, A., Ištvanić, J., and Antonović, A. (2024). Possibilities of liquefied spruce (*Picea abies*) and oak (*Quercus robur*) biomass as an environmentally friendly additive in conventional phenol–formaldehyde resin wood adhesives. *Energies* 17:4456. doi: 10.3390/en17174456

Miranda, I., Gominho, J., Mirra, I., and Pereira, H. (2012). Chemical characterization of barks from *Picea abies* and *Pinus sylvestris* after fractioning into different particle sizes. *Ind. Crop. Prod.* 36, 395–400. doi: 10.1016/j.indcrop.2011.10.035

Mishra, K., Siwal, S. S., Sithole, T., Singh, N., Hart, P., and Thakur, V. K. (2024). Biorenewable materials for water remediation: the central role of cellulose in achieving sustainability. *J. Bioresour. Bioprod.* 9, 253–282. doi: 10.1016/j.jobab.2023.12.002

Mo, Z., Zhang, H., Shahab, A., Chen, J., and Huang, C. (2023). Functionalized metal-organic framework UIO-66 nanocomposites with ultra-high stability for efficient adsorption of heavy metals: kinetics, thermodynamics, and isothermal adsorption. *J. Taiwan Inst. Chem. Eng.* 146:104778. doi: 10.1016/j.jtice.2023.104778

Mosoarca, G., Vancea, C., Popa, S., Boran, S., and Tanasie, C. (2020). A green approach for treatment of wastewater with manganese using wood ash. *J. Chem. Technol. Biotechnol.* 95, 1781–1789. doi: 10.1002/jctb.6376

Munagapati, V. S., Yarramuthi, V., Nadavala, S. K., Alla, S. R., and Abburi, K. (2010). Biosorption of Cu (II), Cd (II) and Pb (II) by *Acacia leucocephala* bark powder: kinetics, equilibrium and thermodynamics. *Chem. Eng. J.* 157, 357–365. doi: 10.1016/j.cej.2009.11.015

Najam, R., and Andrabi, S. M. A. (2016). Adsorption capability of sawdust of *Populus alba* for Pb (II), Zn (II) and Cd (II) ions from aqueous solution. *Desalin. Water Treat.* 57, 29019–29035. doi: 10.1080/19443994.2016.1157039

Natrayan, L., Kaliappan, S., Dheeraj Kumar Reddy, C. N., Karthick, M., Sivakumar, N. S., Patil, P. P., et al. (2022). Development and characterization of carbon-based adsorbents derived from agricultural wastes and their effectiveness in adsorption of heavy metals in waste water. *Bioinorg. Chem. Appl.* 2022:2022. doi: 10.1155/2022/1659855

Ofudje, E. A., Sodiya, E. F., Olanrele, O. S., and Akinwunmi, F. (2023). Adsorption of Cd2+ onto apatite surface: equilibrium, kinetics and thermodynamic studies. *Heliyon* 9:e12971. doi: 10.1016/j.heliyon.2023.e12971

Oguz, E. (2020). Simultaneous removal of lead, copper, cadmium, nickel, and cobalt heavy metal ions from the quinary system by Abies bornmulleriana cones. *Water Sci. Technol.* 82, 3032–3046. doi: 10.2166/wst.2020.547

Orozco, C. I., Freire, M. S., Gómez-Díaz, D., and González-Álvarez, J. (2023). Removal of copper from aqueous solutions by biosorption onto pine sawdust. *Sustain. Chem. Pharm.* 32:101016. doi: 10.1016/j.scp.2023.101016

Rind, I. K., Khuhawar, M. Y., Jahangir, T. M., Memon, N., Habib, A., Lanjwani, M. F., et al. (2024). Risk identification of salts and heavy metals in water by multivariate statistical techniques and GIS based interpolation: a case study of Saeedabad, Sindh, Pakistan. *Reg. Stud. Mar. Sci.* 73:103492. doi: 10.1016/j.rsma.2024.103492

Salamat, A., Ainane, A., Dahbi, L., Khammour, F., Elkouali, M., and Ainane, T. (2017). Valorization the waste of the wood industry (sawdust) and their use as adsorbent material: physicochemical characterization and modeling of optimization sorption using statistical approach. *J. Mater. Environ. Sci.* 9, 201–211.

Sánchez-Moreno, H., García-Rodríguez, L., and Recalde-Moreno, C. (2025). Natural cellulose fibers (*Agave Americana* L. ASPARAGACEAE) impregnated with magnetite nanoparticles as a novel adsorbent of mercury (Hg) in aqueous solutions. *Adsorption* 31, 1–22. doi: 10.1007/s10450-024-00577-1

Šehović, E., Memić, M., Sulejmanović, J., Hameed, M., Begić, S., Ljubijankić, N., et al. (2022). Thermodynamic valorisation of lignocellulosic biomass green sorbents for toxic pollutants removal. *Chemosphere* 307:135737. doi: 10.1016/j.chemosphere.2022.135737

Shukla, S. R., and Pai, R. S. (2005). Adsorption of Cu (II), Ni (II) and Zn (II) on dye loaded groundnut shells and sawdust. *Sep. Purif. Technol.* 43, 1–8. doi: 10.1016/j.seppur.2004.09.003

Simón, D., Palet, C., Costas, A., and Cristóbal, A. (2022). Agro-industrial waste as potential heavy metal adsorbents and subsequent safe disposal of spent adsorbents. *Water* 14:3298. doi: 10.3390/w14203298

Singh, A., Chauhan, S., Varjani, S., Pandey, A., and Bhargava, P. C. (2022). Integrated approaches to mitigate threats from emerging potentially toxic elements: a way forward for sustainable environmental management. *Environ. Res.* 209:112844. doi: 10.1016/j.envres.2022.112844

Soni, V., Soni, V., Sharma, M., Bharti, D., Arora, C., Saxena, R., et al. (2025). "Electronic wastes, its impact on food safety," in Electronic waste. CRC Press, 99–106.

Sreedhar, I., and Reddy, N. S. (2019). Heavy metal removal from industrial effluent using bio-sorbent blends. *SN Appl. Sci.* 1, 1–15. doi: 10.1007/s42452-019-1057-4

Tounsadi, H., Khalidi, A., Abdennouri, M., and Barka, N. (2015). Biosorption potential of *Diplotaxis harra* and *Glebionis coronaria* L. biomasses for the removal of Cd (II) and Co (II) from aqueous solutions. *J. Environ. Chem. Eng.* 3, 822–830. doi: 10.1016/j.jece.2015.03.022

Turchi, M., Galmarini, S., and Lunati, I. (2024). Learning adsorption patterns on amorphous surfaces. *J. Chem. Theory Comput.* 20, 7597–7610. doi: 10.1021/acs.jctc.4c00702

Uddin, M. A., Yuan, X., Wang, L., Yu, H., Wang, H., Yuan, X., et al. (2024). Biomass-derived Organonanomaterials as contrast agents for efficient magnetic resonance imaging. *ACS Appl. Bio. Mater.* 7, 8479–8488. doi: 10.1021/acsabm.4c01295

Wang, X., Meng, L., Hu, M., Gao, L., and Lian, B. (2024). The competitive and selective adsorption of heavy metals by struvite in the Pb(II)-cd(II)-Zn(II) composite system and its environmental significance. *Water Res.* 250:121087. doi: 10.1016/j.watres.2023.121087

Wang, Z., Xu, W., Jie, F., Zhao, Z., Zhou, K., and Liu, H. (2021). The selective adsorption performance and mechanism of multiwall magnetic carbon nanotubes for heavy metals in wastewater. *Sci. Rep.* 11:16878. doi: 10.1038/s41598-021-96465-7

Xu, Z., Chen, S., Yang, B., Zhou, H., Wang, L., Keshta, B. E., et al. (2025). Breakthrough developments in metal-organic frameworks (MOFs) for efficient C4 hydrocarbon adsorption separation. *Chem. Eng. J.* 508:160992. doi: 10.1016/j.cej.2025.160992

Xu, H., Zhou, Q., Yan, T., Jia, X., Lu, D., Ren, Y., et al. (2024). Enhanced removal efficiency of Cd2+ and Pb2+ from aqueous solution by H3PO4–modified tea branch biochar: characterization, adsorption performance and mechanism. *J. Environ. Chem. Eng.* 12:112183. doi: 10.1016/j.jece.2024.112183

Yi, H., Yu, H., Wang, L., Wang, Y., Ouyang, C., and Keshta, B. E. (2024). Microneedle transdermal drug delivery as a candidate for the treatment of gouty arthritis: material structure, design strategies and prospects. *Acta Biomater.* 187, 20–50. doi: 10.1016/j.actbio.2024.08.032

Zhang, M., Li, H., Wang, C., Wang, Z., Liu, D., Yang, T., et al. (2022). Performance enhancement of the poplar wood composites biomimetic mineralized by CaCO3. *ACS Omega* 7, 29465–29474. doi: 10.1021/acsomega.2c03960

Zhu, C., Chu, Z., Ni, C., Chen, Y., Chen, Z., and Yang, Z. (2024). Robust functionalized cellulose-based porous composite for efficient capture and ultra-fast desorption of aqueous heavy metal pollution. *Carbohydr. Polym.* 324:121513. doi: 10.1016/j.carbpol.2023.121513

Zolgharnein, J., Shahmoradi, A., Bagtash, M., Frahani, S. D., and Zolgharnein, P. (2017). Chemometrics optimization for simultaneous adsorptive removal of ternary mixture of Cu (II), Cd (II), and Pb (II) by *Fraxinus* tree leaves. *J. Chemom.* 31:e2935. doi: 10.1002/cem.2935

Glossary

AN - Atomic Number

AR - Atomic Radius (Å) in angstrom

ATR - Attenuated Total Reflectance

As - Arsenic

BET - Brunauer–Emmett–Teller

BSD - Backscattered Electron Detector

BSU - Beni-Suef University

Cd - Cadmium

Ce - Equilibrium concentration (mg/L)

Cf - Final concentration (mg/L)

Ci - Initial concentration (mg/L)

CF - Chemical Formula

CHNS/O - Carbon, Hydrogen, Nitrogen, Sulfur / Oxygen

CI - Covalent Index

Conc - Concentration

Cu - Copper

ddH_2O - Double-distilled Water

DSC - Differential scanning calorimetry

EC - Electron Configuration

EDS - Energy Dispersive X-ray Spectroscopy

Fig - Figure

FTIR - Fourier Transform Infrared

g - Gram

HM/HMs - Heavy Metal/Heavy Metals

Hg - Mercury

HR - Hydrated Radius (Å)

HSAB - Hard-Soft Acid–Base

I - Ionic Strength

ICP-OES - Inductively Coupled Plasma-Optical Emission Spectrometer

IR - Ionic Radius (Å)

Kf - Freundlich constant

KL - Langmuir constant (L/mg)

LC - Lignocellulose

LCB - Lignocellulosic Biomass

Mi - Metal ion

MΩ - Million Ohms

MΩ-cm - Resistivity

$NaNO_3$ - Sodium Nitrate

NSWR - Norway Spruce Wood Residue

pHpzc - Point of Zero Charge

PTEs - Potentially Toxic Elements

Pb - Lead

qe - Equilibrium adsorption capacity (mg/g)

rpm - Round Per Minute

SDGs - Sustainable Development Goals

SDT - Sawdust

SEM - Scanning Electron Microscope / Microscopy

TGA - Thermogravimetric Analysis

WHO - World Health Organization

wt. % - Weight Percentage

WW - Wastewater

XRD - X-Ray Diffraction